Habitability of Stellar Binary Systems

by

ZHAOPENG WANG

Presented to the Faculty of the Graduate School of

The University of Texas at Arlington in Partial Fulfillment

of the Requirements

for the Degree of

DOCTOR OF PHILOSOPHY

THE UNIVERSITY OF TEXAS AT ARLINGTON

August 2017

Copyright © by ZHAOPENG WANG 2017

All Rights Reserved

ACKNOWLEDGEMENTS

I would like to thank my supervising professor Dr. Manfred Cuntz for his invaluable advice during my doctoral studies, and also for constantly motivating and encouraging me.

I wish to thank Dr. Alex Weiss, Dr. Sangwook Park, Dr. Yue Deng and Dr. Zdzislaw Musielak for their interest in my research and for taking time to serve in my dissertation committee.

I am grateful to all the teachers who taught me during the years I spent in school, both in China and in the Unites States.

Moreover, I also would like to thank several of my friends who have helped me throughout my career.

Finally, I would like to express my deep gratitude to my parents for their sacrifice, encouragement and patience.

August 15, 2017

ABSTRACT

Habitability of Stellar Binary Systems

ZHAOPENG WANG, Ph.D.

The University of Texas at Arlington, 2017

Supervising Professor: Manfred Cuntz

A comprehensive approach is provided to the study of habitable zones (HZs) for both S-type and P-type cases of stellar binary systems for both circular and elliptical orbits of the binary components, based on habitability limits for the Sun from previous work. Habitable regions are determined through the consideration of a joint constraint, including the planetary orbital stability and the extent of the radiative habitable zones (RHZs). The HZs are classified based on solar system habitability limits, which also consider different climate models. In this work, the new climate model published by Kopparapu in 2014 is used for RHZ calculation. Comparisons among results from different climate models are made and previous work based on old climate models are introduced. Furthermore, fitting formulae for the quick determination of existence of S-type and P-type Habitable Zones are derived and applied to real systems. The fitting formulae, which are based on Kopparapu's climate model, will be very useful because: (1) the observational uncertainties can be considered in a straightforward manner; (2) the fitting formulae are focusing on main-sequence stars, of which most systems are expected to consist.

TABLE OF CONTENTS

ACKNOWLEDGEMENTS iv

ABSTRACT v

1. Introduction 1

2. Habitability Limits in Stellar Binary System 5

    2.1 Types of Habitability Limits 5

    2.2 Mathematical Approach 6

3. Comparison among Results from Different Climate Models 17

    3.1 Classic Climate Model 17

        3.1.1 Kasting's Work in 1993 17

        3.1.2 Eggl's Work on Binary System 18

        3.1.3 Fitting's on Stellar Flux 20

    3.2 Revised Climate Model 21

        3.2.1 Kopparapu's New Model 21

        3.2.2 Kaltenegger and Haghighipour's Work 21

    3.3 Comparison among Different Climate Models 22

    3.4 Summary and Conclusion 25

4. Fitting Formulae and Constraints for the Existence of

    S-type and P-type Habitable Zones in Binary Systems 51

    4.1 Existence of HZs 51

    4.2 Fitting Procedure 53

    4.3 Applications to Observed Systems 56

        4.3.1 P-type Systems 56

4.3.2 S-type Systems 59
4.3.3 Comparison with Other Work 60
4.4 Summary and Conclusions 61
5. Summary and Future Work 81
Bibliography 83
BIOGRAPHICAL STATEMENT 87

CHAPTER 1

Introduction

As defined by International Astronomical Union (IAU) in 2003, an exoplanet is a celestial body that (a) orbits star(s) or stellar remnant(s); (b) is massive enough to have a hydrostatic equilibrium (nearly round) shape; (c) with masses below the limiting mass for thermonuclear fusion of deuterium; and (d) has cleared its neighboring region of its orbit. In 1992, the first confirmed detection of an exoplanet was announced by Wolszczan & Frail (1992). Since then, thousands of exoplanets were detected, with the number sky-rocketing in the past decade, owing to the successful Kepler mission (Kane et al.l (2016)). Considering the ongoing missions, such as K2, and the planned mission like TESS, it is reasonable to believe more exoplanets would be found in the near future. Thus, it is adequate to perform studies on exoplanets, as well as identifying habitable zones (HZs) of the planet's host stars.

Multiple star systems are known to be common in our Galactic neighborhood based on detailed observations, with binary systems being the majority of them (e.g., Duquennoy & Mayor (1991); Patience et al. (2002); Eggenberger et al. (2004); Raghavan et al. (2006); Raghavan et al. (2010); Roell et al. (2012); Duchêne & Kraus (2013); Milone et al. (2016)). Exoplanets in binary systems may undergo two types of possible orbits (e.g., Dvorak (1982)): S-type orbits stand for planets orbiting one of the binary components, while P-type orbits denote planets orbiting both binary components. Studies also indicate most of binary systems are capable of supporting the formation and the long term stability of terrestrial planets (e.g., Quintana (2008)).

Since 1989, about 80 planet-hosting binary systems have been detected, mostly based on the radial velocity method and transit method. More than 75% of these detected systems hold planets in S-type obits. For instance, HD 114762b, an exoplanet undergoes S-type orbit in the constellation of Coma Berenices, is the first suspected exoplanet around a main-sequence star and the first exoplanet in a binary system. It has been proposed by Latham et al. (1989) and subsequently confirmed in 2012 based on the radial velocity method. A more recent example for S-type exoplanet is K2-29 b (Santerne et al. (2014)). It is a hot Jupiter around a G7V star, with the binary separation between the primary and its K5V companion being about 800 AU. Other S-type examples include HD87646 Ab (Ma et al. (2016)) and Kepler-432 b (Ortiz et al. (2015)). The first detected exoplanet in P-type orbit (also known as circumbinary orbit) is PSR B1620-26 b. Announced in 2003 (Sigurdsson et al. (2003)), it is found to be in a binary system hosting the pulsar B1620-26. Recently, OGLE-2007-BLG-349(AB) b, a planet orbiting two close M dwarfs, has been detected by Bennett et al. (2016) using the microlensing method. Other planets in P-type orbits include Kepler-413 b (Kostov et al. (2014)) and Kepler-453 b (Welsh et al. (2015)).

Exoplanets located within the stellar habitable zones (HZs), which often receive special attention due to their potential for hosting exolife, have also been detected. Proxima Centauri b, which has been detected by Anglada-Escudé et al. (2016), is orbiting within the HZ of Proxima Centauri, the closest star to the Sun. Another amazing case is found for the M8V dwarf star TRAPPIST-1. Seven Earth-sized planets were detected with three of them being considered to be within in the stellar HZ (Gillon et al. (2017)). There are more examples, such as Kepler-62 f (Borucki et al. (2013)), Kepler-452 b (Jon M et al. (2015)). Planets located in HZs of binary system have also been detected, e.g., Kepler-34 (AB) b and Kepler-35 (AB) b (Welsh et al. (2012)).

The habitable zone is a circumstellar region in which a life-supporting planet (or moon) can exist (Huang (1959); Kasting et al. (1993)). Since liquid water is essential to all life forms we know (Fischer et al. (2014)), studies of HZs are aiming at sustaining liquid water on the surface of a terrestrial-mass planet (or moon) (e.g., Huang (1959); Hart (1978); Kasting et al. (1993); Kasting et al. (1993); Underwood et al. (2003); Selsis et al. (2007); Kopparapu et al. (2013)). Focusing on stellar radiation, radiative habitable zones (RHZs) are found to depend on climate model of the planet (Kasting et al. (1993); Kopparapu et al. (2013); Kopparapu et al. (2014)) and effective temperature of the star (Kasting et al. (1993); Kasting et al. (1993); Underwood et al. (2003); Selsis et al. (2007); Kopparapu et al. (2013)).

Focusing on HZs in stellar binary systems, Cuntz (2014) and Cuntz (2015) considered a joint constraint of RHZs (based on Kasting et al. (1993) and Selsis et al. (2007)) and orbital stability. These studies also took into account the eccentricity of binary components, which was found to adversely affect the width of the HZs. Akin to Cuntz (2014) and Cuntz (2015), theoretical background and mathematical approach are introduced in chapter 2.

In previous studies of HZs in stellar binary systems, different climate models and equations for stellar fluxes are applied. For instance, Eggl et al. (2012) used results from Kasting et al. (1993) for S-type systems, Haghighipour et al. (2013) and Kaltenegger et al. (2013) applied results from Kopparapu et al. (2013). In chapter 3, comparisons are made between habitable zones in binary systems from different climate models. Previous work based on different climate model is introduced as well.

Observational data usually has uncertainties, which would affect the habitable limits significantly, or even the sheer existence of habitable zones. Aiming at determining the existence of climatological habitable zones in a straightforward manner with detailed consideration of the observational uncertainties, fitting formulae are

provided in chapter 4, with the use of the updated results on solar habitability limits obtained by Kopparapu et al. (2014). Additionally, both the fitting formulae for S-type and P-type systems are applied to real binary systems.

CHAPTER 2

Habitability Limits in Stellar Binary System

Kasting et al. (1993) published their well-known atmospheric model of Earth-like planets with CO_2, H_2O and N_2 atmospheres for habitability studies. The solar (G2 star) habitable limits are deduced as part of this study. With the consideration of stellar radiation, they also provided the habitable limits and corresponding stellar fluxes for M0 and F0 stars. Kopparapu et al. (2013) updated the model and provided new values for the habitable limits and stellar fluxes (see chapter 3 for details). Based on the concept of single star habitable limits, habitable zones in binary systems can be calculated. In this chapter, the theoretical background and the calculation of HZs are given.

2.1 Types of Habitability Limits

From previous studies, e.g., Kasting et al. (1993), Mischna et al. (2013), Kopparapu et al. (2013), Kopparapu et al. (2014), habitability limits of the solar system are identified based on the radiation from the Sun (see Table 2.1 and Figure 2.1 for details), which defines the RHZs. The meaning of different limits can be stated as follow: the Recent Venus limit is studied as it is believed that Venus does not have liquid water on its surface in the past 1 billion years (Solomon et al. (1991)). The runaway green house effect limit corresponds to the process that the net positive feedback between planetary surface and atmosphere keeps increasing the temperature and boils away the oceans in the end. The moist greenhouse effect limit refers to the case that water starts to escape to space. The first CO_2 condensation limit is studied by Kast-

ing et al. (1993) as they assume the formation of CO_2 clouds would increases albedo of the atmosphere. However, there are studies show that CO_2 clouds could warm a planet, and thus extending the outer limit of habitability (e.g., Forget et al. (1997)). The maximum greenhouse effect limit considers a cloud-free or a 100% clouds CO_2 atmosphere can maintain a 273 K surface temperature. Although seasonal water flows on Mars, the Early Mars limits is studied based on the hypothesis Mars has water bodies on its surface 3.8 billion years before (Pollack et al. (1987)). In this work, I will focus on four limits for Earth-size planet: Recent Venus and Early Mars limits for habitable zone Recent Venus and Early Mars (RVEM), runaway greenhouse effect and maximum greenhouse effect (no cloud) limits for Generalized Habitable Zone (GHZ).

2.2 Mathematical Approach

The mathematical approach is akin to Cuntz (2014, 2015). In binary systems, a planet can either undergoing S-type orbit, which means the planet orbits one star, in P-type orbit, where the planet orbit both planets (Figure 2.2). Thus, habitable zones also can be classified into S-type and P-type habitable zones.

In single star systems, the habitability limits can be calculated as

$$\left(\frac{L/L_{\odot}}{S_{\mathrm{eff},l}}\right)^{0.5} \mathrm{AU} \tag{2.1}$$

Here, L is the luminosity of the star, $L_{\odot}$ is the solar luminosity. $S_{\mathrm{eff},l}$, as a function of effective temperature of binary stars, denoting stellar flux in units of solar constant for different habitability limits (l), can be calculated using the formalism from previous works (see Chapter 3).

For multiple stellar systems with N stars, taking the radiation from all stellar components into account, RHZ can be calculated following the inverse-square law. The key equation reads

$$\sum_{i=1}^{N} \frac{L_i}{S_{\mathrm{eff},il} d_i^2} = L_\odot \tag{2.2}$$

For a binary system with stars of luminosities L_1 and L_2, the equation becomes

$$\frac{L_1}{S_{\mathrm{eff},1l} d_1^2} + \frac{L_2}{S_{\mathrm{eff},2l} d_2^2} = L_\odot \tag{2.3}$$

Here, d_1 and d_2 represent the distances to the binary components. Solar habitability limits, s_l, could be found in Table 2.1.

Using the so-called recast luminosity, which is defined as

$$L_{il}^{'} = \frac{L_i}{L_\odot S_{\mathrm{eff},il}} \tag{2.4}$$

The equation for binary system would become

$$\frac{L_{1l}^{'}}{d_1^2} + \frac{L_{2l}^{'}}{d_2^2} = 1 \tag{2.5}$$

The distance d_1 and d_2 are related to z, the distance from the center of binary system, which yield

$$d_1^2 = a^2 + z^2 + 2az\cos\varphi \tag{2.6}$$

$$d_2^2 = a^2 + z^2 - 2az\cos\varphi \tag{2.7}$$

Here φ is the angle between z and the secondary star with respect to the center of the two stars. Here a is half of the binary separation (also known as binary semi-

major axis), $a_{\rm bin}$. Substituting d_1 and d_2 into the equation for binary system, a quartic equation of z can be obtained after algebraic transformations

$$z^4 + A_2 z^2 + A_1 z + A_0 = 0 \tag{2.8}$$

with

$$\begin{aligned} A_2 &= 2a^2(1 - 2\cos^2\varphi) - (L_{1l}^{'} + L_{2l}^{'}) \\ A_1 &= 2a\cos\varphi(L_{1l}^{'} - L_{2l}^{'}) \\ A_0 &= a^4 - a^2(L_{1l}^{'} + L_{2l}^{'}) \end{aligned} \tag{2.9}$$

The set of solutions of the equation are

$$\begin{aligned} z_1 &= -\frac{1}{2}C - \frac{1}{2}D \\ z_2 &= -\frac{1}{2}C + \frac{1}{2}D \\ z_3 &= +\frac{1}{2}C - \frac{1}{2}E \\ z_4 &= +\frac{1}{2}C + \frac{1}{2}E \end{aligned} \tag{2.10}$$

with

$$\begin{aligned} C &= \sqrt{-2a^2(1 - 2\cos^2\varphi) + (L_{1l}^{'} + L_{2l}^{'}) + y_1} \\ D &= \sqrt{(L_{1l}^{'} + L_{2l}^{'}) + 4a(L_{1l}^{'} - L_{2l}^{'})C^{-1}\cos\varphi - 2a^2(1 - 2\cos^2\varphi) - y_1} \\ E &= \sqrt{(L_{1l}^{'} + L_{2l}^{'}) - 4a(L_{1l}^{'} - L_{2l}^{'})C^{-1}\cos\varphi - 2a^2(1 - 2\cos^2\varphi) - y_1} \end{aligned} \tag{2.11}$$

Here y_1 is a real root (any real root) of the cubic equation

$$y^3 - A_2 y^2 - 4A_0 y + (4A_2 A_0 - A_1^2) = 0 \tag{2.12}$$

which reads

$$y_1 = -\frac{1}{3}\hat{a}_2 + S + T \tag{2.13}$$

with

$$\begin{aligned} S &= \sqrt[3]{R + \sqrt{Q^3 + R^2}} \\ T &= \sqrt[3]{R - \sqrt{Q^3 + R^2}} \\ Q &= \frac{1}{3}\hat{a}_1 - \frac{1}{9}\hat{a}_2^2 \\ R &= -\frac{1}{2}\hat{a}_0 + \frac{1}{6}\hat{a}_1\hat{a}_2 - \frac{1}{27}\hat{a}_2^3 \end{aligned} \tag{2.14}$$

and

$$\begin{aligned} \hat{a}_0 &= 4A_0A_2 - A_1^2 \\ \hat{a}_1 &= -4A_0 \\ \hat{a}_2 &= -A_2 \end{aligned} \tag{2.15}$$

As the planet are supposed to be within the HZ for all the time during the revolution, the inner and outer limits of RHZ can be determined by

$$\mathrm{RHZ}_{\mathrm{out}} = \mathrm{Min}(\mathcal{R}(z, \varphi)) \mid_{\mathrm{out}} \tag{2.16}$$

$$\mathrm{RHZ}_{\mathrm{in}} = \mathrm{Max}(\mathcal{R}(z, \varphi)) \mid_{\mathrm{in}} \tag{2.17}$$

In case of RVEM, the outer limit is regarding to Early Mars and the inner limit is regarding to Recent Venus. They become maximum greenhouse effect (no clouds) and runaway greenhouse effect for GHZ correspondingly. Here $\mathcal{R}$ is the distance measured from the mass center of stars for P-type, and from the one star for S-type. Thus, the RHZs of S-type or P-type orbit, constituting an annulus around each star (S-type) with one star at the center, or both stars with the binary mass center at the center of annulus (P-type).

Binary eccentricity, e_b should also be taken into consideration. To have the planet stays in the HZ for all the time of its revolution, it is necessary to consider the extreme cases, which means periastron for S-type inner limits, and apastron for all the others (Table 2.2).

Furthermore, the orbital stability of the planet needs to be taken into account as well. Fitting formulae for both S-type and P-type planets of binary systems have been developed by Holman & Wiegert (1999) as

$$\frac{a_{\rm cr}}{a_{\rm bin}} = 1.60 + 5.10e_b - 2.22e_b^2 + 4.12\mu - 4.27e_b\mu - 5.09\mu^2 + 4.61e_b^2\mu^2 \tag{2.18}$$

$$\frac{a_{\rm cr}}{a_{\rm bin}} = 0.464 - 0.631e_b - 0.380\mu + 0.586e_b\mu + 0.150e_b^2 - 0.198e_b^2\mu \tag{2.19}$$

with

$$\mu = \frac{M_1}{(M_1 + M_2)} \tag{2.20}$$

The orbital stability limit $a_{\rm cr}$, which depends on the binary separation $a_{\rm bin}$, binary eccentricity e_b and stellar masses M_1 and M_2, is an upper limit for S-type system centered from the primary star, and a lower limit for P-type system measured from the binary mass center.

Combining both constrains, P/PT-type habitable zones are given as

$$\text{Width(P/PT)} = \text{RHZ}_{\rm out} - \text{Max}(\text{RHZ}_{\rm in}, \text{a}_{\rm cr}) \tag{2.21}$$

whereas S/ST-type habitable zone are given as

$$\text{Width(S/ST)} = \text{Min}(\text{RHZ}_{\rm out}, \text{a}_{\rm cr}) - \text{RHZ}_{\rm in} \tag{2.22}$$

Here PT and ST refer to cases that the HZs are smaller than RHZs due to orbital stability requirements.

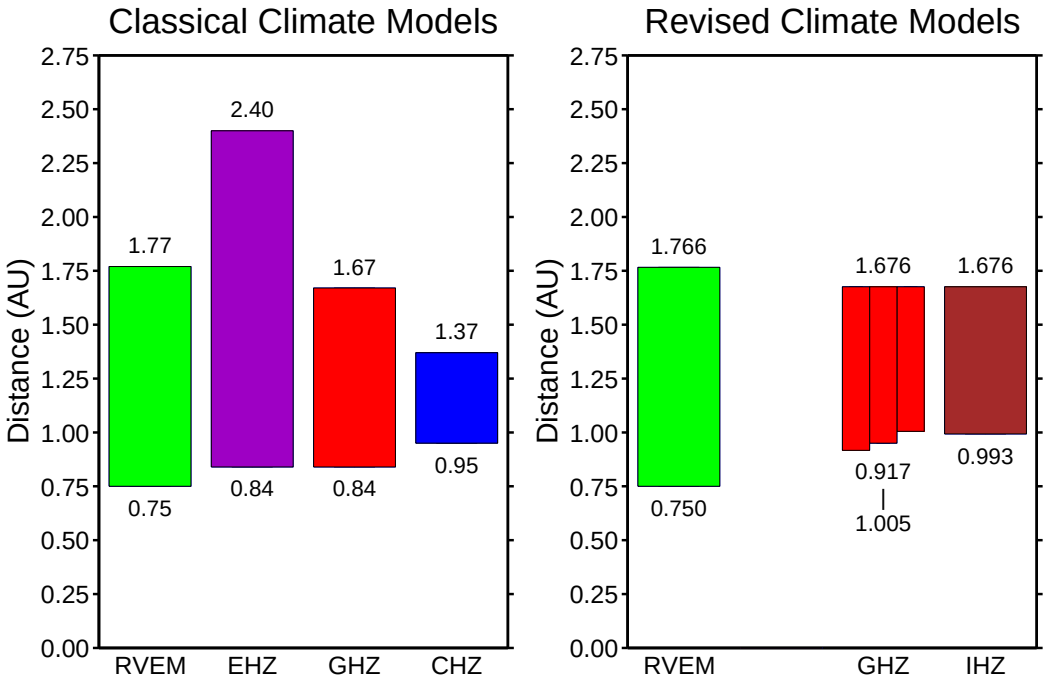

Figure 2.1 Comparison of solar habitability limits from two climate models. Depending on the size of the planet, the inner limit of the GHZ (general habitable zone) for the revised climate model varies from 0.917 to 1.005 AU between the Super-Earth size planet and the Mars-size planet.

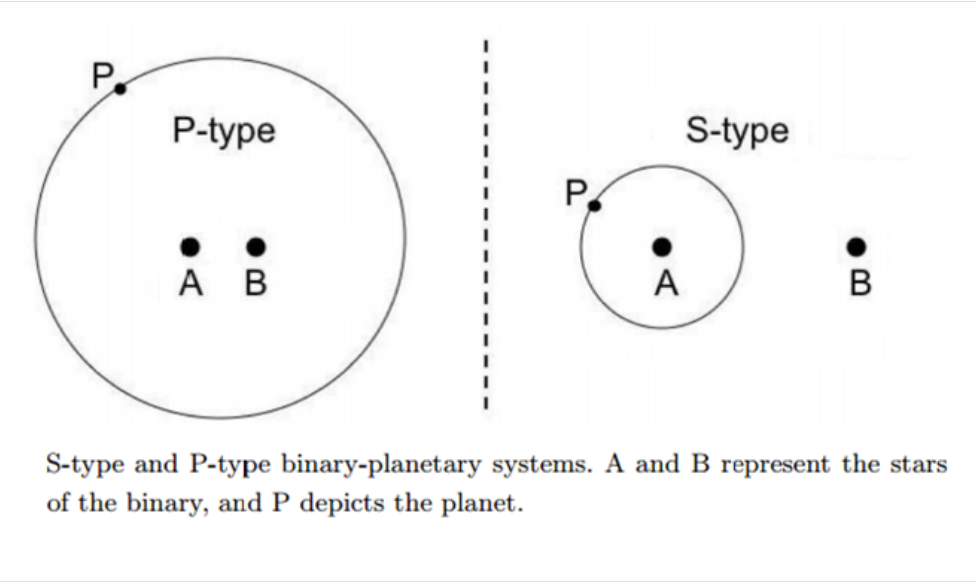

S-type and P-type binary-planetary systems. A and B represent the stars of the binary, and P depicts the planet.

Figure 2.2 S-type and P-type orbits of binary systems. Akin to Haghighipour et al. (2010).

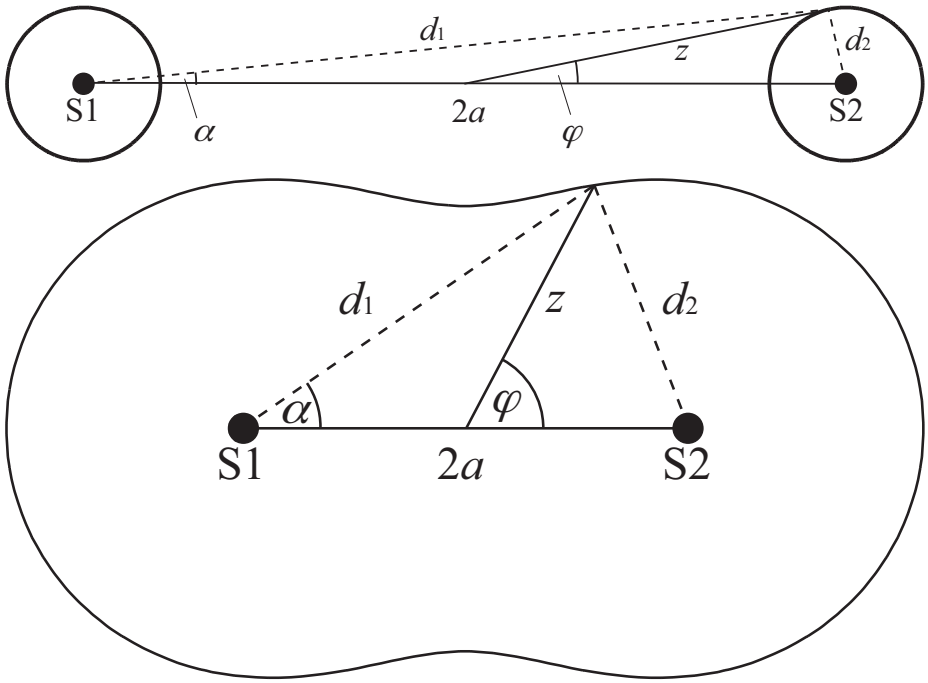

Figure 2.3 Mathematical set-up of S-type (top) and P-type (bottom) habitable zones of binary systems as given by the stellar radiative fluxes. Here $2a$ denotes the semi-major axis $a_{\rm bin}$ of the binary system. It is not necessary for the stars S1 and S2 being identical. Adopted from Cuntz (2014).

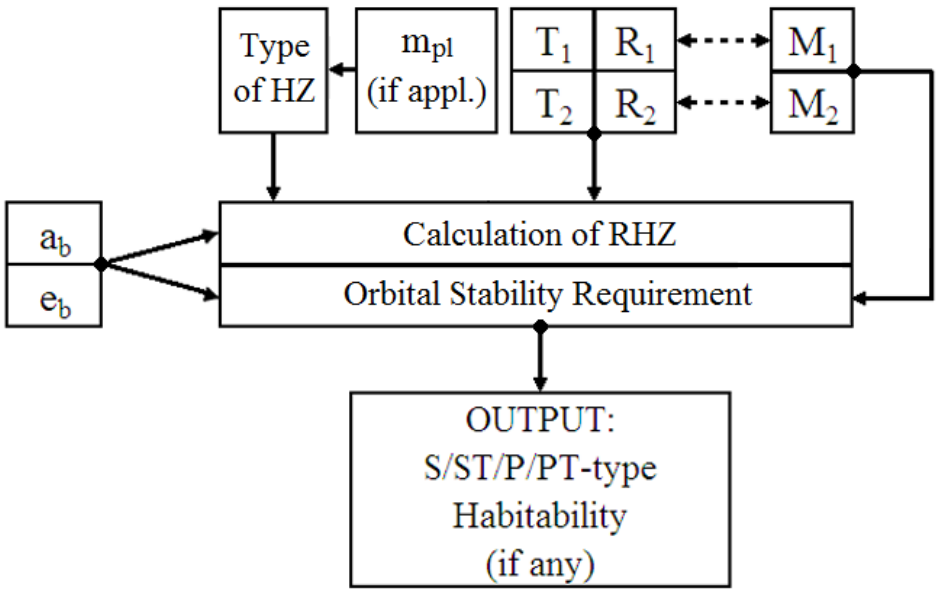

Figure 2.4 Flow diagram of the HZ calculation. Modified after Cuntz (2015).

Table 2.1. Habitability Limits for the Solar system

Description	Indices	Models			
...	ℓ	Kas93		Mis00	Kop1314
...	...	5700 K	5780 K	...	5780 K
...	...	(AU)	(AU)	(AU)	(AU)
Recent Venus	1	0.75	0.77	...	0.750
Runaway greenhouse effect	2	0.84	0.86	...	0.950
Runaway greenhouse effect	2	...	...	...	1.005
Runaway greenhouse effect	2	...	...	...	0.917
Moist greenhouse effect	3	0.95	0.97	...	0.993
Earth-equivalent position	0	0.993	$\equiv$1	...	$\equiv$ 1
First CO_2 condensation	4	1.37	1.40	...	...
Maximum greenhouse effect, no clouds	5	1.67	1.71	...	1.676
Early Mars	6	1.77	1.81	...	1.768
Maximum greenhouse effect, 100% clouds	7	...	...	2.40	...

Note. — Based on Kopparapu et al. (2014), the limit regarding runaway greenhouse effect depends on the size of the planet. For a Mars-size planet (0.1 $M_\oplus$), it is 1.005 AU. It yields 0.950 AU for an Earth-size planet (1.0 $M_\oplus$). In case of super-Earth size planet (5.0 $M_\oplus$), the value becomes 0.917 AU.

Table 2.2. Eccentricity and Habitability Limits

ℓ	s_l	Models		HZ Limits
...	...	S-Type	P-type	...
...	(AU)	(AU)	(AU)	...
1	0.750	$a_b(1-e_b)$	$a_b(1+e_b)$	Recent Venus
2	0.950	$a_b(1-e_b)$	$a_b(1+e_b)$	Runaway greenhouse effect
5	1.676	$a_b(1+e_b)$	$a_b(1+e_b)$	Maximum greenhouse effect
6	1.768	$a_b(1+e_b)$	$a_b(1+e_b)$	Early Mars

Note. — Adopted from Cuntz (2015).

CHAPTER 3

Comparison among Results from Different Climate Models

Kasting et al. (1993) published their climate model with stellar fluxes for M0, G2 (Sun), and F0 main-sequence stars, which allow the calculation of HZs for systems with stars of these spectral types. Underwood et al. (2003) and Selsis et al. (2007) provide different fitting equations for stellar fluxes, which make the calculation of habitability limits applicable to stars of other spectral types. Kopparapu et al. (2013) revised the climate model by Kasting et al. (1993) with chemical planetary atmospheric data from revised data bases and offered updated equations for stellar fluxes. Kopparapu et al. (2014) concluded that the mass of the planet matters to the runaway greenhouse limit, and moreover, updated the coefficients in the stellar flux equations for some habitability limits. In this chapter, I will make comparisons among stellar fluxes from different works, and their effects on habitable zones in binary systems. In addition, I will compare my work to previous works with a focus on habitability limits in binary systems.

3.1 Classic Climate Model

3.1.1 Kasting's Work in 1993

Kasting et al. (1993) published a one-dimensional, cloud-free, climate model for the estimation of habitable zones around our Sun (G2), M0 and F0 main-sequence stars. In this work, they dealt with Earth-like planets with $CO_2/H_2O/N_2$ atmospheres, and assumed that habitability requires the presence of liquid water on the planetary surface. Three pairs of HZ boundaries were introduced. They also com-

puted stellar fluxes corresponding to three types of main sequence stars: M0 (3700 K), G2 (5700 K), and F0 (7200 K). The stellar flux $S_{\rm eff}$, given in unit of solar constant, at different HZ boundaries are shown in Table 3.1.

3.1.2 Eggl's Work on Binary System

In Eggl et al. (2012), habitability limits of S-type orbit in stellar binary systems with a Sun-like primary have been studied based on Kasting et al. (1993), focusing on the influence of secondary with different spectral types on a terrestrial planet orbiting the primary. PHZ, where the planet stays within the Runaway Greenhouse effect limit and Maximum Greenhouse effect limit (GHZ in my thesis work) for all times were studied using inequalities, which are also based on inverse-square law. For outer limit (Maximum Greenhouse effect limit), it is

$$1 \leq \frac{L_1}{B_1}\frac{1}{(a_p(1+e_p^{\rm max}))^2} + \frac{L_2}{B_2}\frac{1}{(a_{\rm bin}(1+e_b)+a_p(1+e_p^{\rm max}))^2} \tag{3.1}$$

And for inner limit, the Runaway Greenhouse effect limit, the inequality reads

$$1 \geq \max\begin{cases} \frac{L_1}{A_1}\frac{1}{(a_p(1-e_p^{\rm max}))^2} + \frac{L_2}{A_2}\frac{1}{(a_{\rm bin}(1-e_b)-a_p(1-e_p^{\rm max}))^2} \\ \frac{L_1}{A_1}\frac{1}{(a_p(1+e_p^{\rm max}))^2} + \frac{L_2}{A_2}\frac{1}{(a_{\rm bin}(1-e_b)-a_p(1+e_p^{\rm max}))^2} \end{cases} \tag{3.2}$$

Here $a_{\rm bin}$ denotes the semi-major axis of binary system, with a_p being the semi-major axis of the planet which orbits the primary star. $e_p^{\rm max}$ is the maximum eccentricity of the planet. Moreover, L_1 and L_2 are the luminosities of the primary and secondary stars correspondingly, with A and B are the limiting radiation values, depend on spectral type of the stars, for the inner (A) and outer (B) border of the HZ in units of solar constants, which are the same as stellar fluxes in Table 3.1. Eggl et al. (2012) also considered cases that parts of the planetary orbit lie outside the HZ, and thus defined their Extended Habitable Zone (EHZ) and Averaged Habitable Zone (AHZ).

For EHZ, most of the planet's orbit remains inside the HZ boundaries and thus makes the planet still considered to be habitable, yields

$$\langle \mathrm{S_{eff}} \rangle_{\mathrm{t}} + \sigma \leq \mathrm{A} \wedge \langle \mathrm{S_{eff}} \rangle_{\mathrm{t}} - \sigma \geq \mathrm{B} \tag{3.3}$$

where σ^2 denotes the insolation variance. In case of the AHZ, the time-averaged insolation on the planet is supposed to be within the limits

$$B \geq \langle \mathrm{S_{eff}} \rangle_{\mathrm{t}} \geq \mathrm{A} \tag{3.4}$$

The secondary star is treated as a perturbator. Additionally, the eccentricity of the planetary orbit has been taken into account for the calculation of HZs. Therefore, $e_p^{\max}$ is introduced as the maximum eccentricity the planet can acquire. Eggl et al. (2012) derived an equation for $e_p^{\max}$ as

$$e_p^{\max} = e_p^{\mathrm{sp}} + e_p^{\mathrm{sec}} \tag{3.5}$$

where e_p^{sp} denotes the amplitude of short-period terms and e_p^{sec} the planetary eccentricity's secular amplitude, which yield

$$e_p^{\mathrm{sp}} = \alpha \left(\frac{15}{64} \frac{\beta}{X^{5/3}} \frac{(4+11e_b^2)}{(1-e_b^2)^{5/2}} + \frac{11}{4} \frac{1}{X^2} \frac{(1+e_b)^3}{(1-e_b^2)^3} + \frac{3}{4} \frac{1}{X^3} \frac{(1+e_b)^4(6+11e_b)}{(1-e_b^2)^{9/2}} \right) \tag{3.6}$$

$$e_p^{\mathrm{sec}} = e_b \beta \left(\frac{5}{4} \frac{\alpha}{X^{1/3}} \frac{(3+2e_b^2)}{(1-e_b^2)^{1/2}} - \frac{2}{5} \gamma X^{1/3} (1-e_b^2)^{1/2} + \frac{2}{5} X^{2/3} (1-e_b^2) \right)^{-1} \tag{3.7}$$

with

$$\alpha = \frac{m_2}{M}$$

$$\beta = \frac{m_1 - m_p}{(m_1+m_p)^{2/3} M^{1/3}}$$

$$\gamma = \frac{m_1 m_p M^{1/3}}{m_2 (m_1+m_p)^{4/3}}$$

$$M = m_1 + m_2 + m_p$$

$$X = \left(\frac{m_1+m_p}{M} \right)^{1/2} \left(\frac{a_b}{a_p} \right)^{3/2}$$

Here m_p is the mass of planet and m_1, m_2 are the stellar mass of primary and secondary.

3.1.3 Fitting's on Stellar Flux

In Kasting et al. (1993), stellar fluxes are provided for standard M0, G2 and F0 main-sequence stars. However, these are just a subset of the stars that exist. In order to apply the climate model to main-sequence stars with different spectral types, fitting equations are derived and the two most widely used were given by Underwood et al. (2003) and Selsis et al. (2007).

Underwood et al. (2003) studied the evolution of habitable zones during stellar lifetimes based on the climate model considered by Kasting et al. (1993). Parabolic equations are used to fit the stellar fluxes, in unit of solar constant, provided in the model:

$$S_{\rm eff} = a_y T_{\rm eff}^2 + b_y T_{\rm eff} + c_y \tag{3.8}$$

Here $T_{\rm eff}$ is the stellar effective temperature. The coefficients are listed in Table 3.2.

Selsis et al. (2007) studied the habitable zone of Gliese 581, a red dwarf, based on the climate model from Kasting et al. (1993). For that study, they provided a formalism for stellar fluxes, which are the fitting equations also used in Cuntz (2014) for classic climate model. The stellar fluxes, in unit of solar constant, read

$$S_{\rm eff} = (s_l - a_z T_{**} - b_z T_{**}^2)^{-2} \tag{3.9}$$

Here s_l represents different habitability limits from Kasting et al. (1993) (See Table 3.1). However, the Recent Venus limit is different, which is given as 0.72 AU in Selsis et al. (2007). $T_{**} = T_{\rm eff} - 5700$ K. The coefficients a_z and b_z depended on the type of habitability limit. For inner limits, i.e., $s_l < 1$, $a_z = 2.7619 \times 10^{-5}$ and $b_z =$

3.8095×10^{-9}. For outer limits, i.e., $s_l > 1$, in case of outer limits, $a_z = 1.3786 \times 10^{-4}$ and $b_z = 1.4286 \times 10^{-9}$.

3.2 Revised Climate Model

3.2.1 Kopparapu's New Model

After the article of Kasting et al. (1993) was published, their climate model is widely used for habitability studies since many decades. Kopparapu et al. (2013) published the new results of solar habitability limits based on their new climate model, which is a revised version of the one of Kasting et al. (1993). This updated 1D radiative convective, cloud-free climate model has new CO_2 and H_2O absorption coefficients, taken from new data bases, which are the crucial improvements. Furthermore, an updated equation for stellar flux calculation is given as

$$S_{\text{eff}} = S_{\text{eff}\odot} + aT_* + bT_*^2 + cT_*^3 + dT_*^4 \tag{3.10}$$

Here $T_* = T_{\text{eff}} - 5780$ K. See Table 3.3 for coefficients. Kopparapu et al. (2014) took the planetary mass into account, with detailed consideration of N_2 background pressure. They found that the runaway greenhouse limit also depends on the mass of planet. Additionally, the coefficients in the equation for stellar flux were updated. See Table 3.4 for the new coefficients for Earth-size planet.

3.2.2 Kaltenegger and Haghighipour's Work

Kaltenegger et al. (2013) and Haghighipour et al. (2013) also studied habitability in P-type and S-type binary systems based on the climate model derived by Kopparapu et al. (2013). Although P-type and S-type were studied separately, the equations as used for habitability limits calculation are the same. A coordinate system with the primary star at the center is used (Figure 3.1).

The total flux $F_{\rm Pl}$ received by a planet in a binary system is assumed to be

$$F_{\rm Pl}(f, T_{\rm Pr}, T_{\rm Sec}) = W_{\rm Pr}(f, T_{\rm Pr})\frac{L_{\rm Pr}(T_{\rm Pr})}{r^2_{\rm Pl-Pr}} + W_{\rm Sec}(f, T_{\rm Sec})\frac{L_{\rm Sec}(T_{\rm Sec})}{r^2_{\rm Pl-Sec}} \tag{3.11}$$

Here $T_{\rm Pr}$ and $T_{\rm Sec}$ denote the effective temperature of the two stars. $L_{\rm Pr}$ and $L_{\rm Sec}$ are the luminosities of the binary components, which are related to the stellar temperatures. $r_{\rm Pl-Pr}$ and $r_{\rm Pl-Sec}$ represent the distances from the planet to the primary and the secondary stars. However, the effect of cloud fraction, f, is not studied in Kopparapu et al. (2013) and Kopparapu et al. (2014). The spectral weight factor $W(f, T)$ is normalized to the flux of the Sun. It is obtained after an algebraic transformation of the equation given by Kopparapu et al. (2013). The result yields

$$W_i(f, T_i) = [1 + \alpha(T_i)s_l^2]^{-1} \tag{3.12}$$

with

$$\alpha(T_i) = aT_i + bT_i^2 + cT_i^3 + dT_i^4 \tag{3.13}$$

The coefficients used are the same as in Kopparapu et al. (2013) given in Table 3.3.

The habitability limits for binary systems can be calculated by

$$W_{\rm Pr}(f, T_{\rm Pr})\frac{L_{\rm Pr}(T_{\rm Pr})}{l^2_{x-\rm Bin}} + W_{\rm Sec}(f, T_{\rm Sec})\frac{L_{\rm Sec}(T_{\rm Sec})}{r^2_{\rm Pl-Sec}} = \frac{L_{\rm Sun}}{s_l^2} \tag{3.14}$$

with $l_{x-\rm Bin}$ denoting the inner and outer limits for different HZs, with distances measured from the primary star.

3.3 Comparison among Different Climate Models

Underwood et al. (2003) (Und03), Selsis et al. (2007) (Sel07), Kopparapu et al. (2013) (Kop13) and Kopparapu et al. (2014) (Kop14) offered different equations for stellar fluxes calculations. Comparisons are made between these fitting equations (See Figure 3.2). Next, I am going to check the maximum difference in stellar fluxes at different temperatures.

In case of the Recent Venus limit, the largest percent difference in stellar fluxes at 3700 K is 22.62%, arise from Kop14 and Sel07. At 7200 K, stellar fluxes between Und03 and Sel07 have a percent difference of 10.78%. For a G2 star (5780 K), the percent difference between Und03 and Sel07 is 9.22%.

Considering the limit regarding the runaway greenhouse effect, the percent difference at 3700 K between Sel07 and Kop13 is 51.48%. Und03 and Kop13 give a percent difference of 38.91% at 7200 K, and 29.82% at 5780 K, respcetively.

There is a 21.94% percent difference between Und03 and Kop14 at 3700 K for the limit regarding to maximum greenhouse effect. Sel07 and Kop14 have a percent difference of 2.30% at 7200 K. For a star with an effective temperature of 5780 K, the percent difference between Und03 and Kop14 is 2.40%.

The percent difference of Early Mars limit is 20.94% between Sel07 and Kop14 at 3700 K. For 7200 K, Kop14 and Kop13 yield a percent difference of 0.95%. For a solar type star (5780 K), the percent difference is 1.29%, between Und03 and Kop13 (or Kop14).

In summary, the stellar fluxes for the inner limits of RVEM and GHZ have large differences between classic climate model (Underwood et al. (2003) and Selsis et al. (2007)) and the revised climate models (Kopparapu et al. (2013) and Kopparapu et al. (2014)). The outer limits match each other very well at higher temperatures. Although the percent difference are larger at lower temperatures, the absolute difference is small. Thus, I expect that only the inner limits, especially the limit regarding to runaway greenhouse effect, would yield large differences between classic climate model and revised climate model. Equations for stellar fluxes calculation from Sel07 and Kop14 are focused for HZs comparison, as they are most recent ones for each climate model (see Figures 3.3-3.12 and Tables 3.5-3.12.).

Focusing on equal mass P-type systems with $M_1 = 1.00M_\odot$, $M_2 = 1.00M_\odot$ and $a_{\rm bin} = 0.20$ AU, the inner limits of GHZ are 1.355 AU at $e_b = 0.0$ and 1.369 AU at $e_b = 0.5$ for Kop14. The limits become 1.197 AU and 1.212 AU for Sel07, respectively. The GHZ outer limits at $e_b = 0.0$ are 2.368 AU for Kop14, and 2.344 AU for Sel07. At $e_b = 0.5$, the outer limits of GHZ are 2.365 AU and 2.341 AU, respectively. For RVEM, the inner limits are 1.075 AU for Kop14 and 1.030 AU for Sel07 at $e_b = 0.0$. At $e_b = 0.5$, the values are 1.092 AU and 1.047 AU, respectively. The outer limits for Kop14 are 2.506 AU at $e_b = 0.0$ and 2.503 AU at $e_b = 0.5$. The values change to 2.486 AU and 2.483 AU for Sel07, respectively.

For a non-equal mass P-type cases with $M_1 = 1.25M_\odot$, $M_2 = 0.75M_\odot$ and $a_{\rm bin} = 0.20$ AU, the inner limits of GHZ are 1.526 AU for Kop14 and 1.362 AU for Sel07 at $e_b = 0.0$. The values become 1.565 AU and 1.402 AU at $e_b = 0.5$, correspondingly. At $e_b = 0.0$, the outer limits of GHZ are 2.554 AU for Kop14 and 2.523 AU for Sel07. The limits become 2.525 AU and 2.494 AU at $e_b = 0.5$, respectively. For inner limits of RVEM, Kop14 has 1.216 AU at $e_b = 0.0$ and 1.256 AU at $e_b = 0.5$. Sel07 has 1.172 AU and 1.213 AU, respectively. In case of outer limits, the values are 2.704 AU for Kop14 and 2.681 AU for Sel07 at $e_b = 0.0$. At $e_b = 0.5$, the values are 2.675 AU and 2.652 AU, correspondingly.

Considering S-type system with $M_1 = 1.00M_\odot$, $M_2 = 1.00M_\odot$ and $a_{\rm bin} = 20.0$ AU, Kop14 has 0.952 AU at e_b =0.0 and 0.956 AU at e_b =0.5 for GHZ inner limit. Sel07 has 0.839 AU and 0.841 AU, correspondingly. The outer limits of GHZ are 1.681 AU for Kop14 and 1.664 AU for Sel07 at $e_b = 0.0$. The limits are 1.678 AU and 1.661 AU at $e_b = 0.5$, respectively. The inner limits of RVEM are 0.751 AU for Kop14 and 0.718 AU for Sel07 at $e_b = 0.0$, with the outer limits being 1.779 AU and 1.765 AU, respectively. At $e_b = 0.5$, the values become 0.753 AU and 0.720 AU, 1.776 AU and 1.762 AU, correspondingly.

Keep $a_{\text{bin}} = 20.0$ AU, for an S-type system with $M_1 = 1.25M_\odot$, $M_2 = 0.75M_\odot$, the GHZ inner limits at $e_b = 0.0$ are 1.356 AU for Kop14 and 1.209 AU for Sel07. Changing e_b to 0.5, the limits become 1.358 AU and 1.211 AU, respectively. Kop14 has 2.367 AU at $e_b = 0.0$ and 2.365 AU at $e_b = 0.5$ for GHZ outer limits. Sel07 has 2.340 AU and 2.339 AU, correspondingly. In case of RVEM, the inner limits are 1.070 AU for Kop14 and 1.033 AU for Sel07 at $e_b = 0.0$. The limits are 1.071 AU and 1.034 AU at $e_b = 0.5$, correspondingly. For RVEM outer limits, Kop14 has 2.504 AU at $e_b = 0.0$ and 2.502 AU at $e_b = 0.5$. Sel07 has 2.487 AU and 2.486 AU, correspondingly.

3.4 Summary and Conclusion

In this chapter, several studies aiming at HZs in binary systems are introduced, with all of them based on the inversed-square law. Eggl et al. (2012) studied habitability limits of GHZ for S-type systems, using climate model from Kasting et al. (1993). Eggl et al. (2012) have taken the maximum eccentricity of the planetary orbit into account. They also proposed the idea that the planet could be temporarily outside of the GHZ, which can still be considered habitable. Kaltenegger et al. (2013) and Haghighipour et al. (2013) applied the revised planetary climate model from Kopparapu et al. (2013), with the coordinate systems centered at the primary star for both P-type and S-type systems. Cuntz (2014, 2015) adopted stellar fluxes fitting equations from Selsis et al. (2007) with detailed consideration of the binary eccentricity. In his work, the coordinate system is centered right at the half-way point between two stellar components. In addition, Cuntz (2014, 2015) derived analytical solution for stellar HZs. In my work, I follow the mathematical approach of Cuntz (2014, 2015); moreover, different climate models are applied. (In chapter 4, Kopparapu et al. (2014) is used.)

Comparisons are made between different climate models as well. In case of the stellar fluxes, it is found that stellar fluxes for the outer limits yield relatively small differences, especially for stars with high effective temperatures. Differences among stellar fluxes of the inner limits are much greater. The HZs based on different climate model are compared as well. All inner limits, and some outer limits for systems consisting of stars with low effective temperatures are found to have larger differences between the different climate models. This behavior is also mirrored in the stellar fluxes.

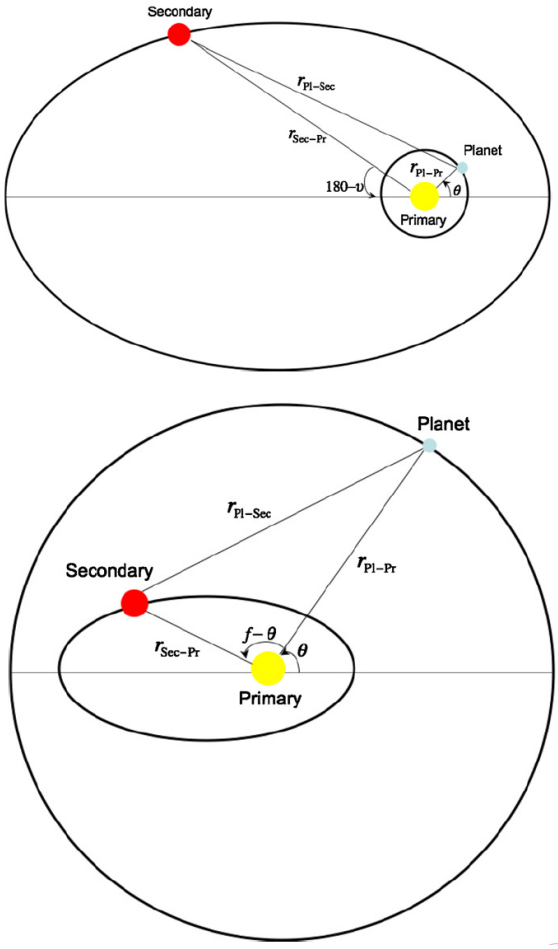

Figure 3.1 System setup as used by Kaltenegger et al. (2013) and Haghighipour et al. (2013).

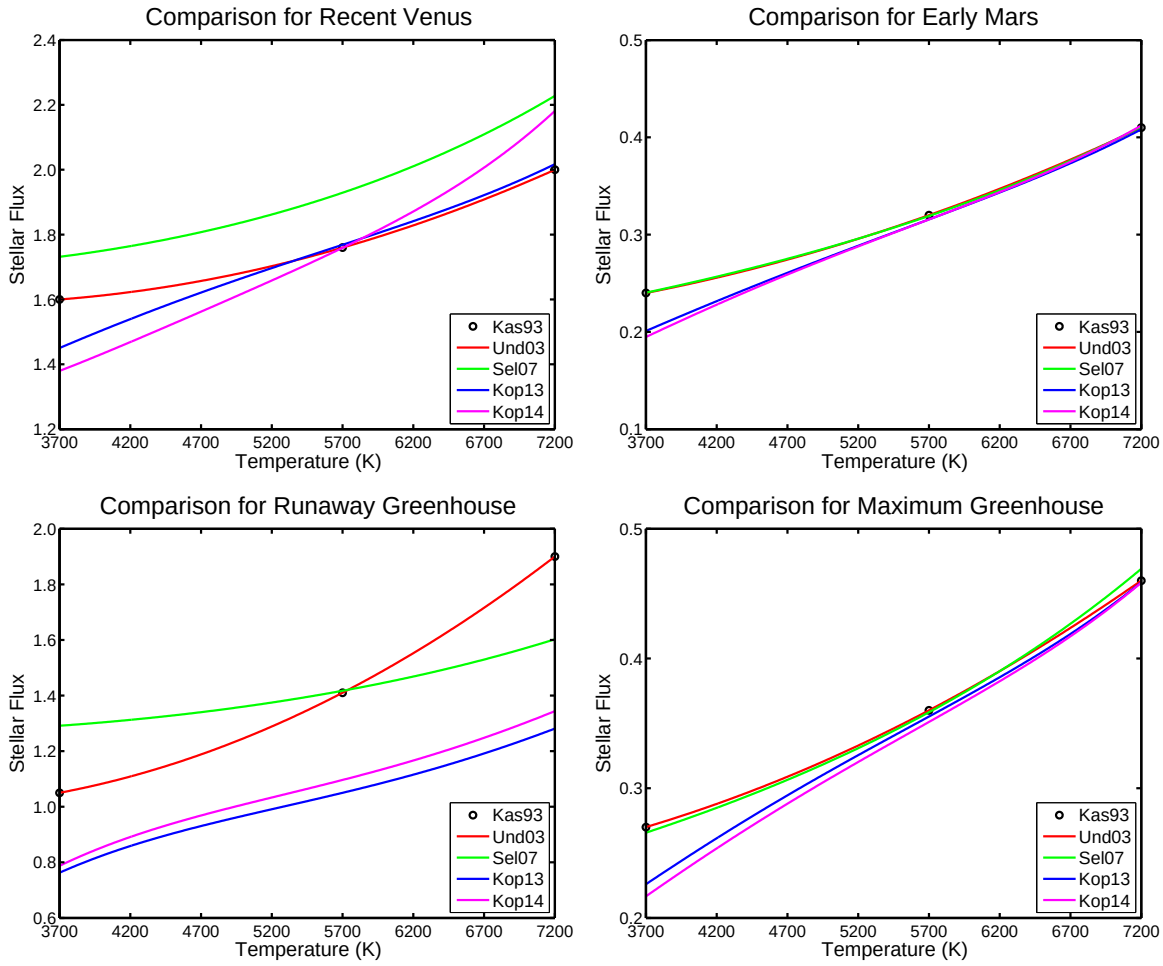

Figure 3.2 Stellar flux comparison as given by Kasting et al. (1993), Underwood et al. (2003), Selsis et al. (2007) and Kopparapu et al. (2013, 2014).

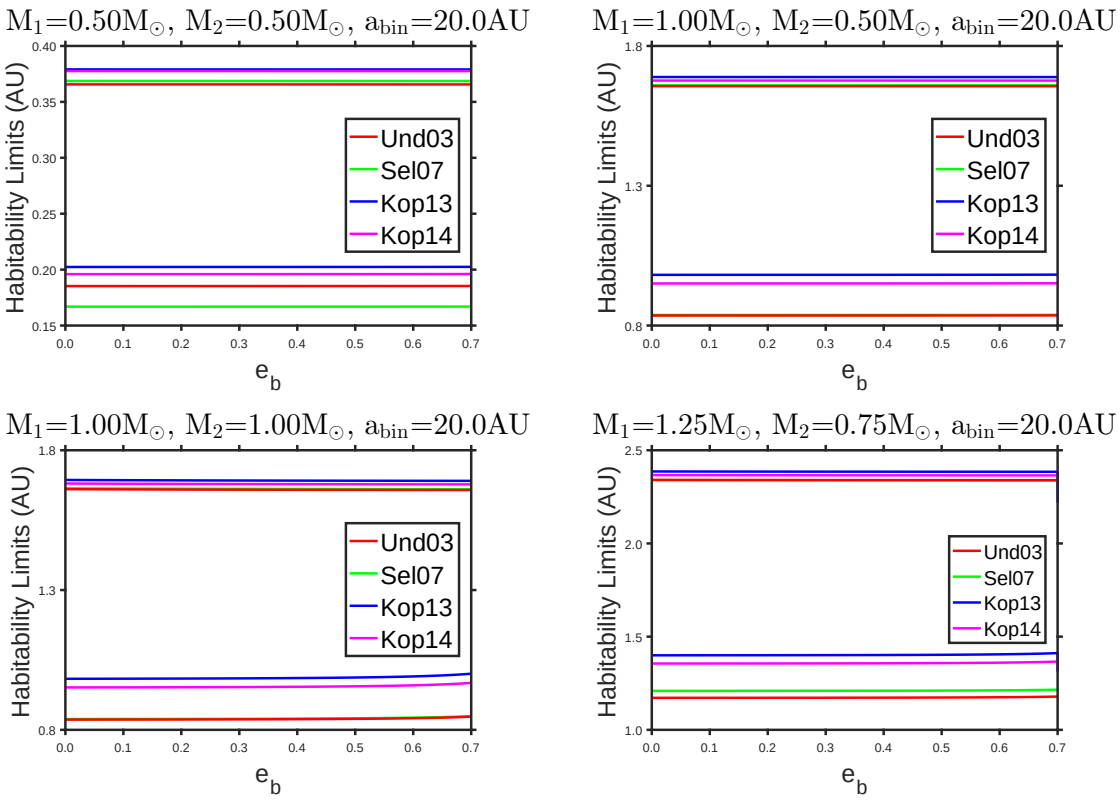

Figure 3.3 S-type GHZ inner and outer limits comparisons. The binary separation is assumed as $a_{\rm bin} = 20.0$ AU.

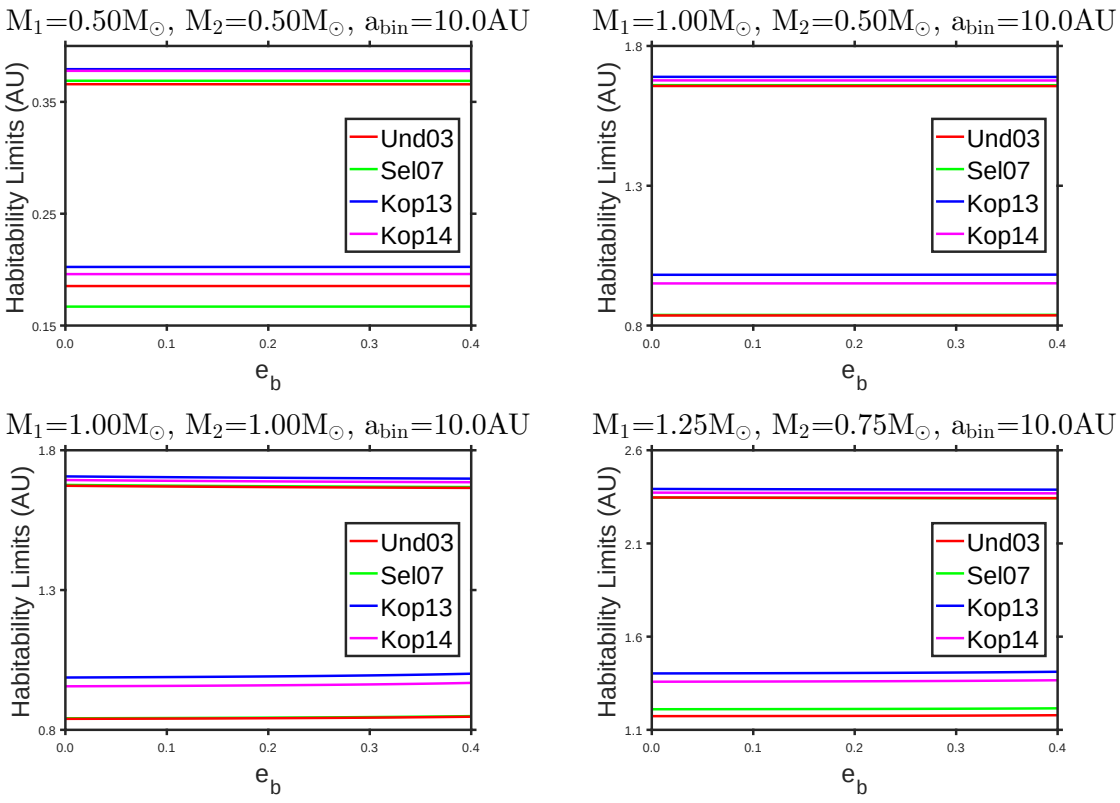

Figure 3.4 S-type GHZ inner and outer limits comparisons. The binary separation is assumed as $a_{\text{bin}} = 10.0$ AU.

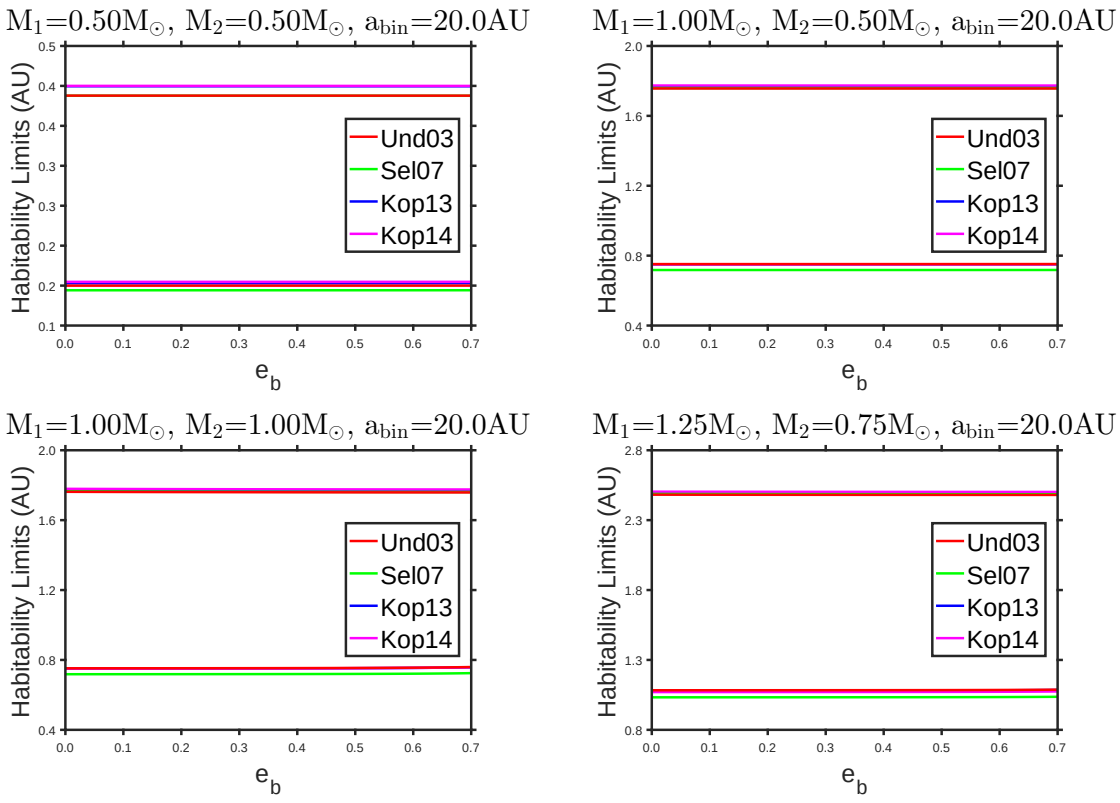

Figure 3.5 S-type RVEM inner and outer limits comparisons. The binary separation is assumed as $a_{\text{bin}} = 20.0$ AU.

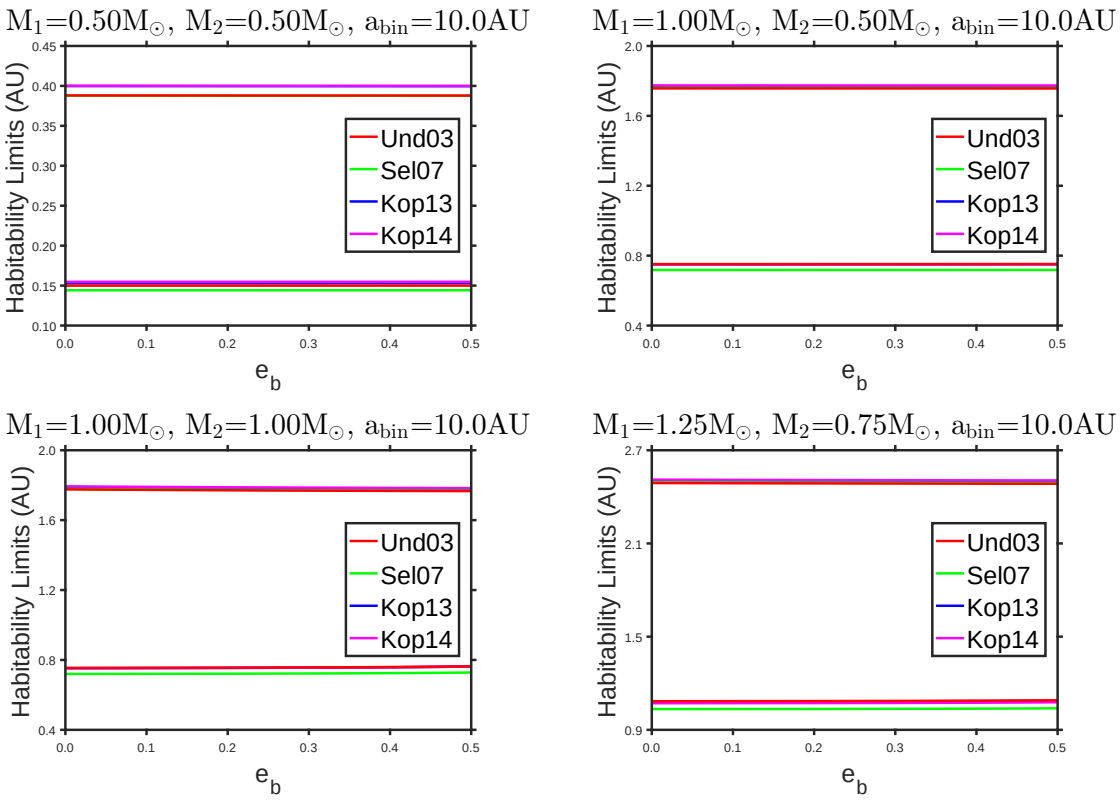

Figure 3.6 S-type RVEM inner and outer limits comparisons. The binary separation is assumed as $a_{\text{bin}} = 10.0$ AU.

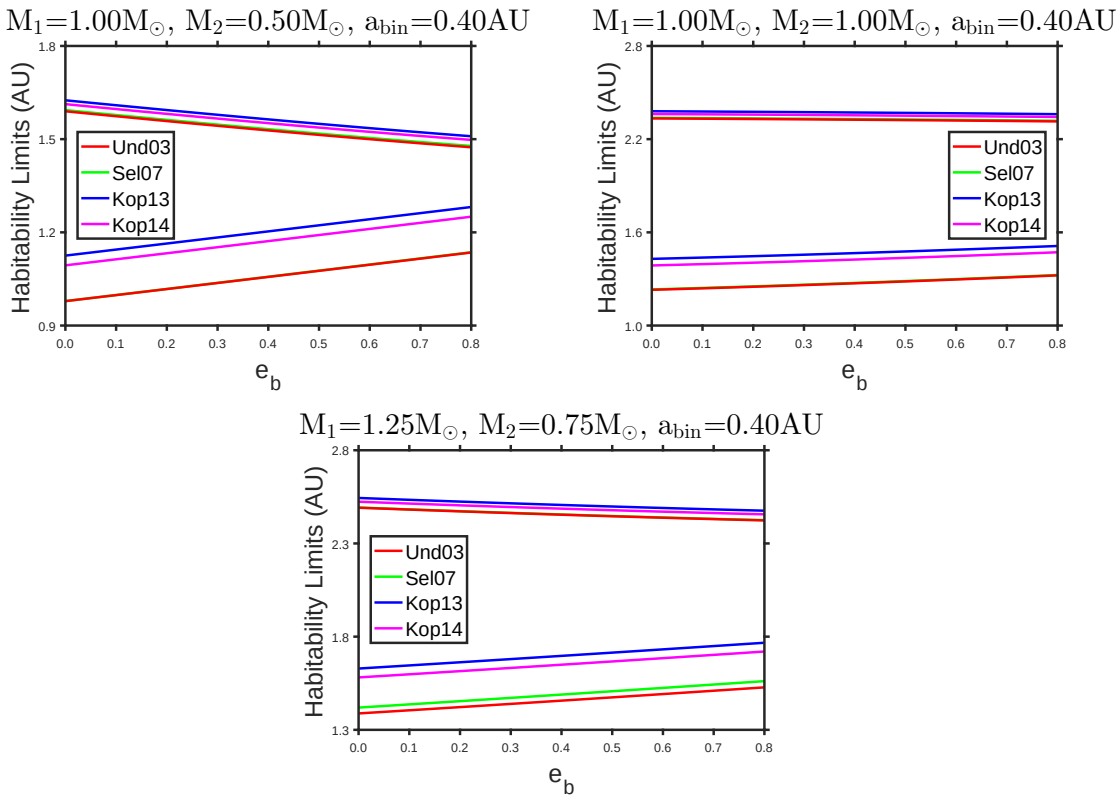

Figure 3.7 P-type GHZ inner and outer limits comparisons. The binary separation is assumed as $a_{\text{bin}} = 0.40$ AU.

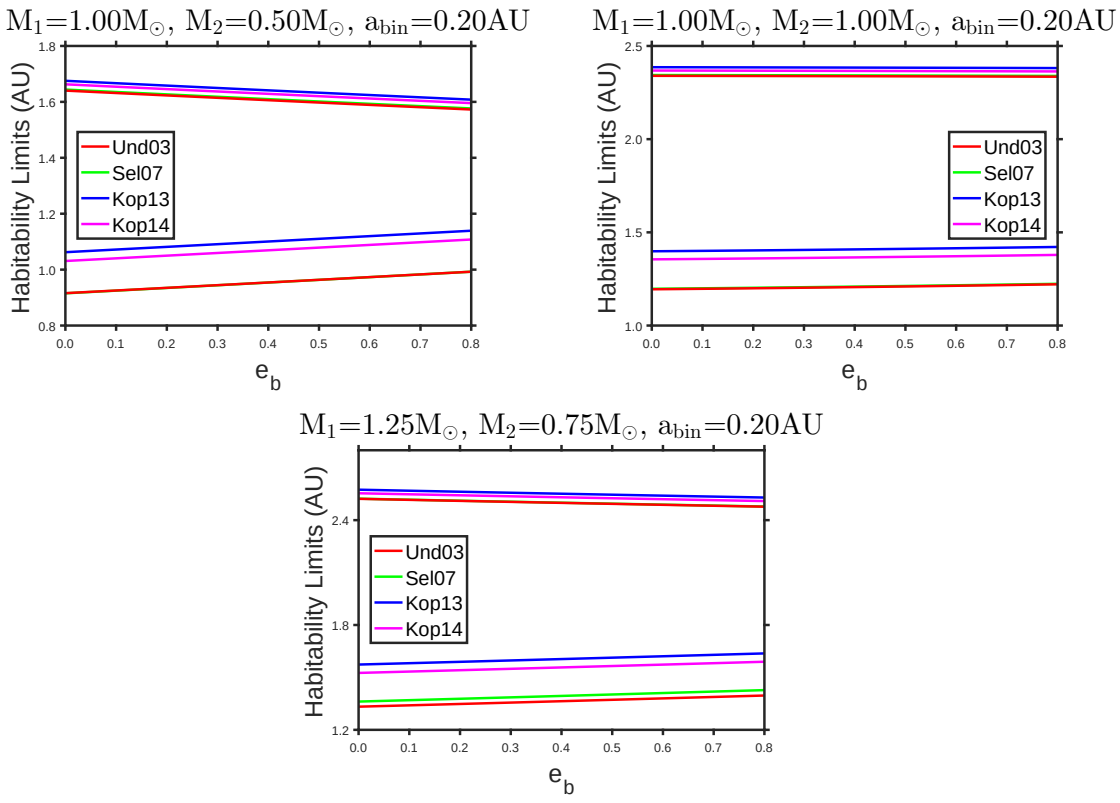

Figure 3.8 P-type GHZ inner and outer limits comparisons. The binary separation is assumed as $a_{\rm bin} = 0.20$ AU.

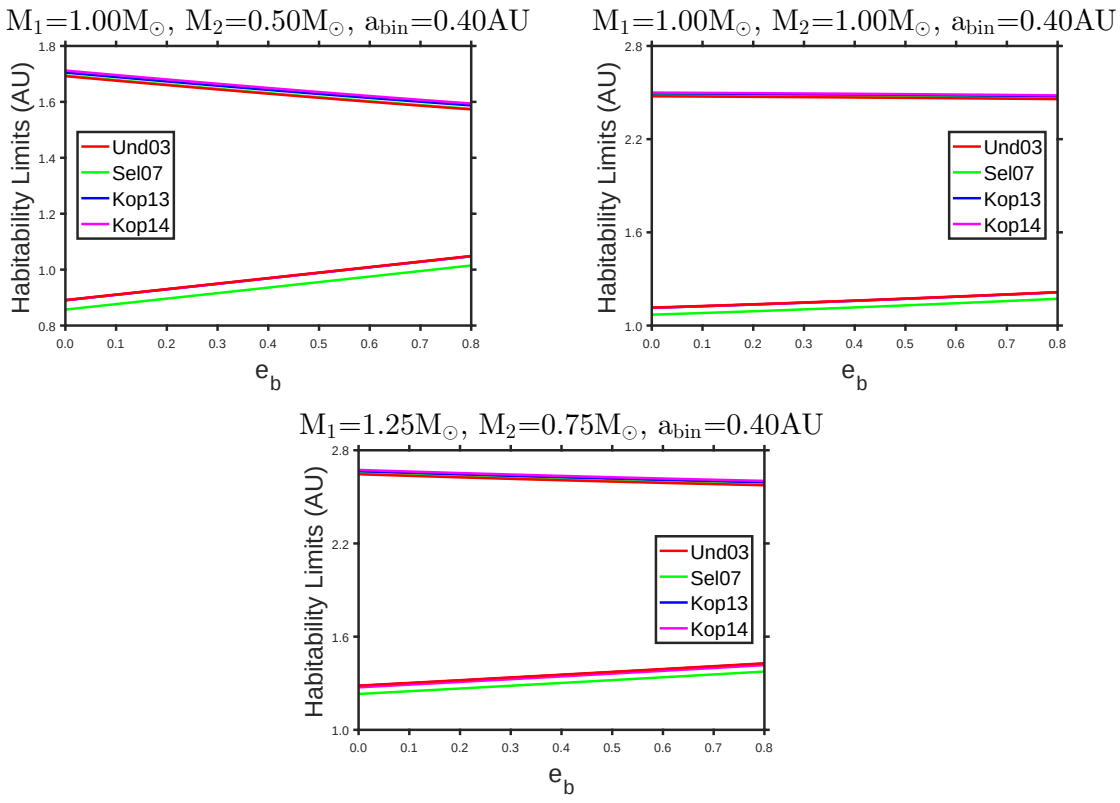

Figure 3.9 P-type RVEM inner and outer limits comparisons. The binary separation is assumed as $a_{\text{bin}} = 0.40$ AU.

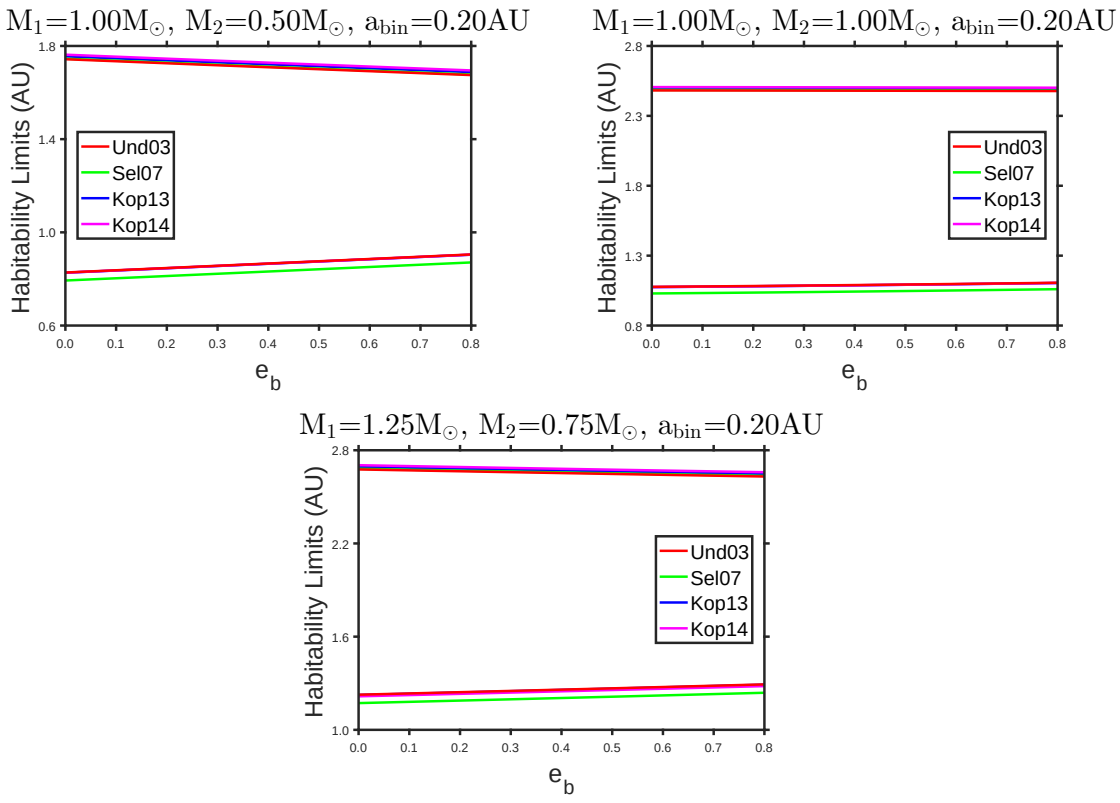

Figure 3.10 P-type RVEM inner and outer limits comparisons. The binary separation is assumed as $a_{\text{bin}} = 0.20$ AU.

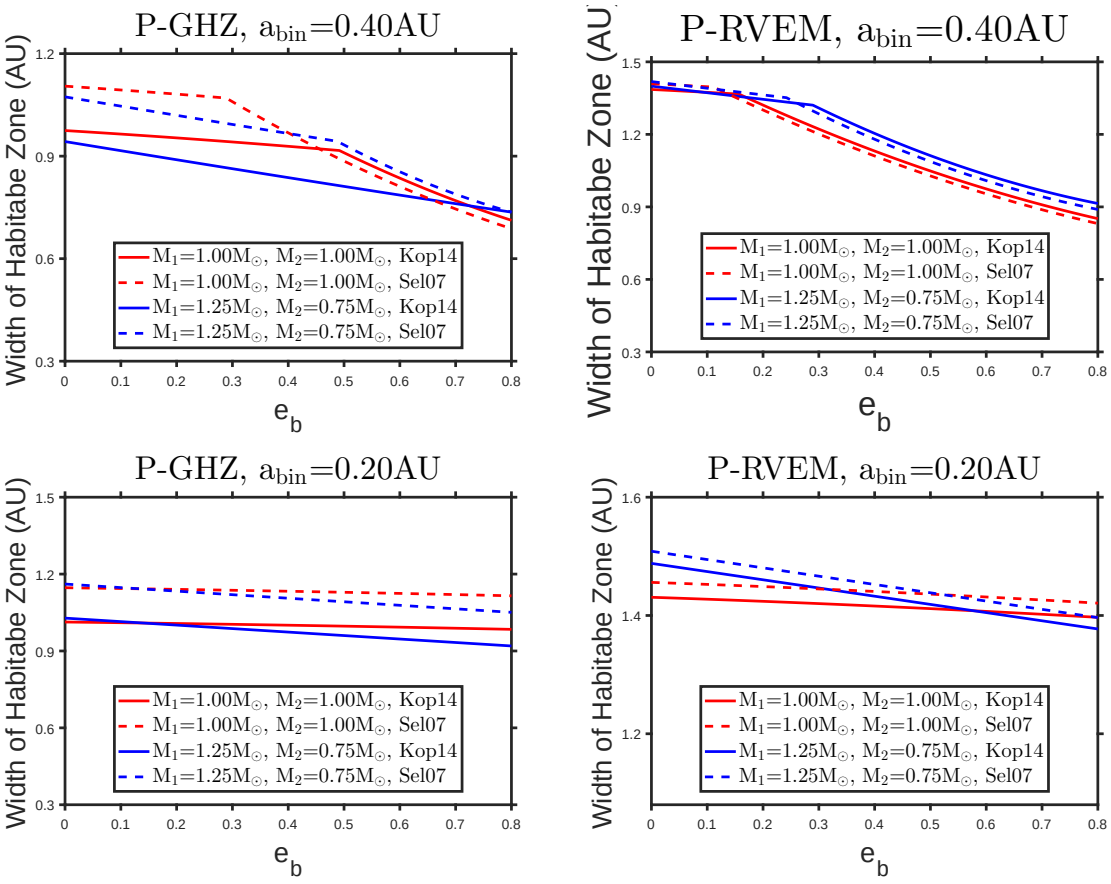

Figure 3.11 Width of P-type HZs.

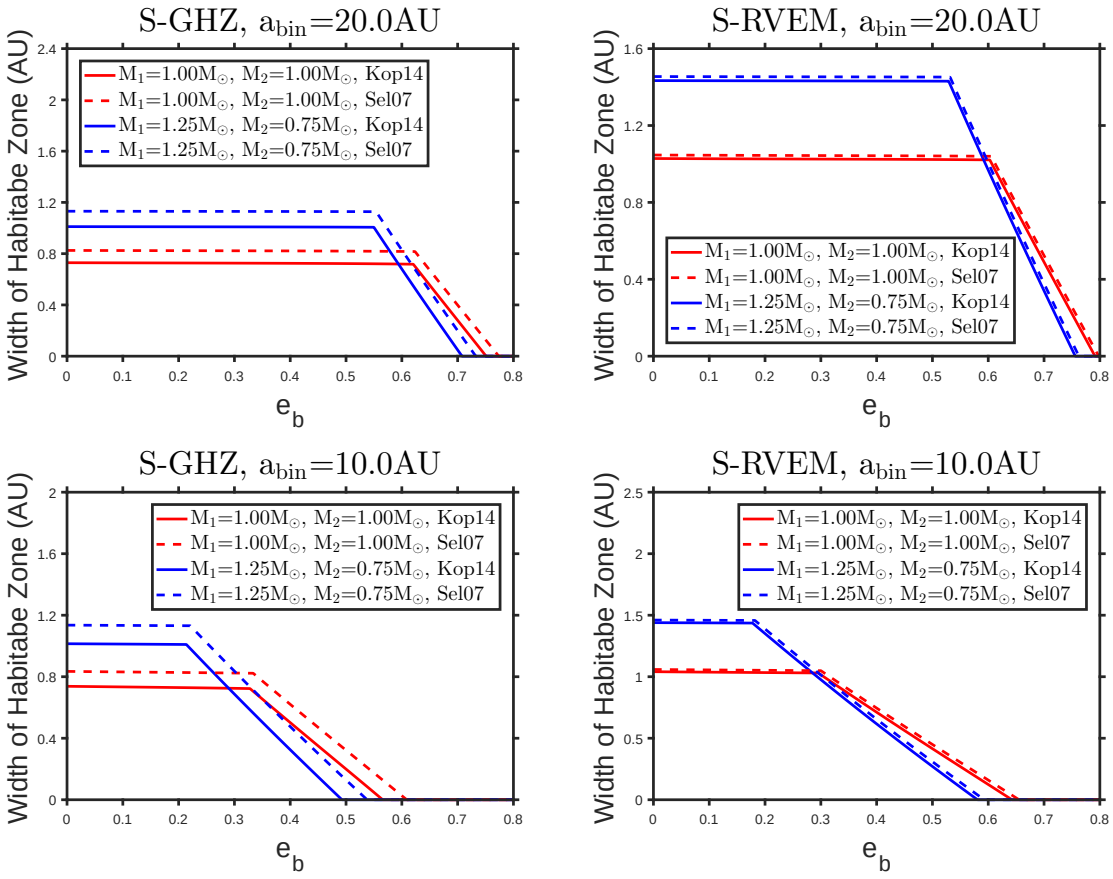

Figure 3.12 Width of S-type HZs.

Table 3.1. Stellar Flux and Habitability Limits from Kasting et al. (1993)

Stellar type	M0		G2		F0	
$T_{\rm eff}$(K)	3700		5700		7200	
$M/M_{\odot}$	0.5		1.0		1.3	
$L/L_{\odot}$	0.06		1.0		4.3	
Habitablility Limits	$S_{\rm eff}$	s_l	$S_{\rm eff}$	s_l	$S_{\rm eff}$	s_l
Recent Venus	1.60	0.19	1.76	0.75	2.00	1.80
Runaway greenhouse	1.05	0.24	1.41	0.84	1.90	1.85
Water loss	1.00	0.25	1.10	0.95	1.25	2.28
First CO2 condensation	0.46	0.36	0.53	1.37	0.61	3.26
Maximum greenhouse	0.27	0.47	0.36	1.67	0.46	3.76
Early Mars	0.24	0.50	0.32	1.77	0.41	3.98

Note. — The luminosities L, stellar masses M, effective temperature $T_{\rm eff}$, stellar fluxes $S_{\rm eff}$ and the corresponding habitability limits s_l from Kasting et al. (1993). Recent Venus fluxes and Early Mars fluxes, for both M0 and F0 stars, are derived from their water loss fluxes and maximum greenhouse fluxes correspondingly, by multiplying the ratio of the flux values of the G2 star.

Table 3.2. Coefficents from Underwood et al. (2003)

Coefficents	Recent Venus	Runaway greenhouse	Water los	First CO_2 condensation	Maximum greenhouse	Early Mars
a_y	2.286×10^{-8}	4.190×10^{-8}	1.429×10^{-8}	5.238×10^{-9}	6.190×10^{-9}	5.714×10^{-9}
b_y	-1.349×10^{-4}	-2.139×10^{-4}	-8.429×10^{-5}	-1.424×10^{-5}	-1.319×10^{-5}	-1.371×10^{-5}
c_y	1.786	1.268	1.116	0.4410	0.2341	0.2125

Table 3.3. Coefficents from Kopparapu et al. (2013) (Erratum)

	GHZ		RVEM	
	Runaway Greenhouse	Maximum Greenhouse	Recent Venus	Early Mars
$l_{x-\mathrm{Sun}}$ (AU)	0.97	1.67	0.75	1.77
Flux (Solar Flux @ Earth)	1.0385	0.3507	1.7763	0.3207
a	1.2456×10^{-4}	5.9578×10^{-5}	1.4335×10^{-4}	5.4471×10^{-5}
b	1.4612×10^{-8}	1.6707×10^{-9}	3.3954×10^{-9}	1.5275×10^{-9}
c	-7.6345×10^{-12}	-3.0058×10^{-12}	-7.6364×10^{-12}	-2.1709×10^{-12}
d	-1.7511×10^{-15}	-5.1925×10^{-16}	-1.1950×10^{-15}	-3.8282×10^{-16}

Table 3.4. Coefficents from Kopparapu et al. (2014)

	GHZ		RVEM	
	Runaway Greenhouse	Maximum Greenhouse	Recent Venus	Early Mars
Flux (Solar Flux @ Earth)	1.107	0.356	1.776	0.320
a	1.332×10^{-4}	6.171×10^{-5}	2.136×10^{-4}	5.547×10^{-5}
b	1.580×10^{-8}	1.698×10^{-9}	2.533×10^{-8}	1.526×10^{-9}
c	-8.308×10^{-12}	-3.198×10^{-12}	-1.332×10^{-11}	-2.874×10^{-12}
d	-1.931×10^{-15}	-5.575×10^{-16}	-3.097×10^{-15}	-5.011×10^{-16}

Table 3.5. Percent difference for $M_1 = 1.25M_\odot$, $M_2 = 0.75M_\odot$

	GHZ		RVEM	
e_b	Runaway Greenhouse	Maximum Greenhouse	Recent Venus	Early Mars
0.0	11.445%	1.123%	3.563%	0.655%
0.1	11.445%	1.123%	3.565%	0.654%
0.2	11.453%	1.122%	3.566%	0.654%
0.3	11.461%	1.122%	3.568%	0.653%
0.4	11.473%	1.122%	3.571%	0.653%
0.5	11.496%	1.122%	3.576%	0.653%
0.6	11.543%	1.121%	3.588%	0.653%
0.7	11.674%	1.121%	3.616%	0.652%

Note. — Percent differences between S-type habitability limits calculated based on Selsis et al. (2007) and Kopparapu et al. (2014) are given. Here e_b is the eccentricity of the binary system. The binary separation is assumed as $a_{\rm bin} = 20.0$ AU. At higher eccentricity, the habitable zones do not exist due to planetary orbital stability requirements.

Table 3.6. Percent difference for $M_1 = 1.25M_\odot$, $M_2 = 0.75M_\odot$

	GHZ		RVEM	
e_b	Runaway Greenhouse	Maximum Greenhouse	Recent Venus	Early Mars
0.0	11.496%	1.130%	3.576%	0.663%
0.1	11.515%	1.128%	3.581%	0.662%
0.2	11.543%	1.127%	3.588%	0.660%
0.3	11.590%	1.127%	3.598%	0.659%
0.4	11.674%	1.126%	3.616%	0.658%
0.5	–	–	3.651%	0.657%

Note. — Percent differences between S-type habitability limits calculated based on Selsis et al. (2007) and Kopparapu et al. (2014) are given. Here e_b is the eccentricity of the binary system. The binary separation is assumed as $a_{\rm bin} = 10.0$ AU. At higher eccentricity, the habitable zones do not exist due to planetary orbital stability requirements.

Table 3.7. Percent difference for $M_1 = 1.00M_\odot$, $M_2 = 1.00M_\odot$

	GHZ		RVEM	
e_b	Runaway Greenhouse	Maximum Greenhouse	Recent Venus	Early Mars
0.0	12.631%	1.028%	4.449%	0.818%
0.1	12.638%	1.027%	4.451%	0.817%
0.2	12.649%	1.026%	4.453%	0.816%
0.3	12.665%	1.026%	4.457%	0.816%
0.4	12.691%	1.025%	4.462%	0.816%
0.5	12.737%	1.025%	4.473%	0.815%
0.6	12.831%	1.024%	4.493%	0.815%
0.7	13.076%	1.024%	4.543%	0.815%

Note. — Percent differences between S-type habitability limits calculated based on Selsis et al. (2007) and Kopparapu et al. (2014) are given. Here e_b is the eccentricity of the binary system. The binary separation is assumed as $a_{\rm bin} = 20.0$ AU. At higher eccentricity, the habitable zones do not exist due to planetary orbital stability requirements.

Table 3.8. Percent difference for $M_1 = 1.00M_\odot$, $M_2 = 1.00M_\odot$

	GHZ		RVEM	
e_b	Runaway Greenhouse	Maximum Greenhouse	Recent Venus	Early Mars
0.0	12.737%	1.040%	4.473%	0.829%
0.1	12.775%	1.038%	4.481%	0.826%
0.2	12.831%	1.035%	4.493%	0.825%
0.3	12.920%	1.034%	4.512%	0.823%
0.4	13.076%	1.032%	4.543%	0.822%
0.5	13.386%	1.031%	4.603%	0.821%
0.6	–	–	4.741%	0.820%

Note. — Percent differences between S-type habitability limits calculated based on Selsis et al. (2007) and Kopparapu et al. (2014) are given. Here e_b is the eccentricity of the binary system. The binary separation is assumed as $a_{\rm bin} = 10.0$ AU. At higher eccentricity, the habitable zones do not exist due to planetary orbital stability requirements.

Table 3.9. Percent difference for $M_1 = 1.25M_\odot$, $M_2 = 0.75M_\odot$

	GHZ		RVEM	
e_b	Runaway Greenhouse	Maximum Greenhouse	Recent Venus	Early Mars
0.0	10.789%	1.240%	3.397%	0.890%
0.1	10.642%	1.245%	3.336%	0.898%
0.2	10.497%	1.250%	3.276%	0.906%
0.3	10.354%	1.255%	3.218%	0.914%
0.4	10.215%	1.260%	3.162%	0.922%
0.5	10.078%	1.264%	3.108%	0.929%
0.6	9.944%	1.267%	3.055%	0.936%
0.7	9.813%	1.270%	3.004%	0.943%
0.8	9.684%	1.273%	2.954%	0.950%

Note. — Percent differences between P-type habitability limits calculated based on Selsis et al. (2007) and Kopparapu et al. (2014) are given. Here e_b is the eccentricity of the binary system. The binary separation is assumed as $a_{\rm bin} = 0.40$ AU.

Table 3.10. Percent difference for $M_1 = 1.25M_\odot$, $M_2 = 0.75M_\odot$

	GHZ		RVEM	
e_b	Runaway Greenhouse	Maximum Greenhouse	Recent Venus	Early Mars
0.0	11.353%	1.219%	3.652%	0.858%
0.1	11.277%	1.223%	3.619%	0.862%
0.2	11.202%	1.226%	3.585%	0.866%
0.3	11.127%	1.230%	3.552%	0.870%
0.4	11.052%	1.233%	3.519%	0.874%
0.5	10.978%	1.237%	3.487%	0.878%
0.6	10.904%	1.240%	3.455%	0.882%
0.7	10.830%	1.243%	3.423%	0.886%
0.8	10.757%	1.246%	3.392%	0.891%

Note. — Percent differences between P-type habitability limits calculated based on Selsis et al. (2007) and Kopparapu et al. (2014) are given. Here e_b is the eccentricity of the binary system. The binary separation is assumed as $a_{\rm bin} = 0.20$ AU.

Table 3.11. Percent difference for $M_1 = 1.00M_\odot$, $M_2 = 1.00M_\odot$

	GHZ		RVEM	
e_b	Runaway Greenhouse	Maximum Greenhouse	Recent Venus	Early Mars
0.0	11.769%	1.029%	4.031%	0.818%
0.1	11.619%	1.031%	3.962%	0.819%
0.2	11.463%	1.033%	3.890%	0.820%
0.3	11.302%	1.035%	3.818%	0.822%
0.4	11.137%	1.037%	3.746%	0.823%
0.5	10.970%	1.039%	3.673%	0.825%
0.6	10.801%	1.041%	3.601%	0.826%
0.7	10.631%	1.044%	3.530%	0.828%
0.8	10.462%	1.046%	3.460%	0.830%

Note. — Percent differences between P-type habitability limits calculated based on Selsis et al. (2007) and Kopparapu et al. (2014) are given. Here e_b is the eccentricity of the binary system. The binary separation is assumed as $a_{\rm bin} = 0.40$ AU.

Table 3.12. Percent difference for $M_1 = 1.00M_\odot$, $M_2 = 1.00M_\odot$

	GHZ		RVEM	
e_b	Runaway Greenhouse	Maximum Greenhouse	Recent Venus	Early Mars
0.0	12.373%	1.024%	4.325%	0.814%
0.1	12.327%	1.024%	4.301%	0.814%
0.2	12.277%	1.025%	4.277%	0.815%
0.3	12.224%	1.025%	4.250%	0.815%
0.4	12.167%	1.026%	4.222%	0.815%
0.5	12.107%	1.026%	4.193%	0.816%
0.6	12.045%	1.027%	4.163%	0.816%
0.7	11.980%	1.027%	4.131%	0.817%
0.8	11.912%	1.028%	4.099%	0.817%

Note. — Percent differences between P-type habitability limits calculated based on Selsis et al. (2007) and Kopparapu et al. (2014) are given. Here e_b is the eccentricity of the binary system. The binary separation is assumed as $a_{\rm bin} = 0.20$ AU.

CHAPTER 4

Fitting Formulae and Constraints for the Existence of S-type and P-type Habitable Zones in Binary Systems

Exoplanets in the HZ always tend to receive significant attention from the scientific community and the public owing to their potential of harboring life. Thus, it is reasonable to choose systems which have HZs for detailed simulations and other studies. In this chapter, fitting formulae for the quick determination of HZs are presented, which also can a straightforward view with the consideration of observational uncertainties.

4.1 Existence of HZs

Various sets of binary systems, encompassing both systems of equal and non-equal masses, have been studied to examine the existence of their HZs based on the radiative criterion, as described by the stellar luminosities, as well as the orbital stability criterion for system planets. Information on the adopted stellar parameters, chosen for cases of theoretical main-sequence stars, are given in Table 4.1. Regarding the stellar HZs, I focus on the GHZ and RVEM (see Chapter 2) and consider stars with masses M_1 and M_2 of 0.50 $M_\odot$, 0.75 $M_\odot$, 1.00 $M_\odot$, and 1.25 $M_\odot$; see Figures 4.1 to 4.4 for details.

For systems of masses $M_1 = M_2 = 1.0\ M_\odot$, in case of $e_b = 0$, the semi-major axis $a_{\rm bin}$ is required to be smaller than 0.97 AU for the P/PT-type GHZ to exist and smaller than 1.03 AU for the P/PT-type RVEM to exist. Regarding S/ST-type HZs, $a_{\rm bin}$ needs to be larger than 3.72 AU and larger than 2.93 AU for the GHZ and RVEM

to exist, respectively. Larger eccentricities barely affect the existence of P/PT-type HZs; however, they notably affect the existence of the S/ST-type HZs. For $e_b = 0.50$, $a_{\rm bin}$ is required to be larger than 8.44 AU and larger than 6.66 AU for S/ST-type GHZ and RVEM to exist, respectively.

Different values for the existence of P/PT and S/ST-type HZs are obtained for other kinds of equal-mass systems. For systems with masses $M_1 = M_2 = 0.50\ M_\odot$, in case of $e_b = 0$, $a_{\rm bin}$ is required to be smaller than 0.22 AU for the P/PT-type GHZ to exist and smaller than 0.23 AU for the P/PT-type RVEM to exist. Regarding S/ST-type HZs, $a_{\rm bin}$ needs to be larger than 0.76 AU and larger than 0.60 AU for the GHZ and RVEM to exist, respectively. Again, larger eccentricities barely affect the existence of P/PT-type HZs; however, they impact the existence of the S/ST-type HZs, as expected. For $e_b = 0.50$, $a_{\rm bin}$ is required to be larger than 1.74 AU and larger than 1.37 AU for S/ST-type GHZ and RVEM to exist, respectively.

I also investigated non-equal mass systems, which generally are considered more significant than equal-mass systems. In systems of $M_1 = 1.00\ M_\odot$ and $M_2 = 0.50\ M_\odot$, $a_{\rm bin}$ is required to be smaller than 0.81 AU and smaller than 0.86 AU for the P/PT-type GHZ and RVEM, respectively, in case of $e_b = 0$. Furthermore, $a_{\rm bin}$ needs to be larger than 2.83 AU and larger than 2.23 AU to allow for the existence of the S/ST-type GHZ and RVEM, respectively. Again, high eccentricities barely affect the existence of P/PT-type HZs; however, they impact the existence of the S/ST-type HZs as already pointed out for equal-mass systems. For $e_b = 0.50$, $a_{\rm bin}$ is required to be larger than 6.78 AU and larger than 5.35 AU for S/ST-type GHZ and RVEM to exist, respectively.

Moreover, I also considered systems of $M_1 = 1.25\ M_\odot$ and $M_2 = 0.75\ M_\odot$. The case of $e_b = 0$ requires $a_{\rm bin}$ to be smaller than 1.20 AU and smaller than 1.27 AU for the P/PT-type GHZ and RVEM, respectively. Regarding S/ST-type HZs, $a_{\rm bin}$

is required to be larger than 4.36 AU for the GHZ and larger than 3.41 AU for the RVEM regarding $e_b = 0$. Furthermore, $a_{\rm bin}$ is required to be larger than 10.17 AU for the GHZ and larger than 8.03 AU for the RVEM and $e_b = 0.50$. Even higher values of $a_{\rm bin}$ are needed for both the GHZ and RVEM in case of eccentricities beyond 0.50.

In summary, the existence of P/PT-type HZs is barely affected by the eccentricity of the stellar system and solely controlled by M_1 and M_2 (or, say, L_1 and L_2). However, relatively large semi-major axes $a_{\rm bin}$ are required for the existence of S/ST-type HZs in highly eccentric systems. Large values of $a_{\rm bin}$ always ensure S/ST-type HZs, as in this case, the stellar habitable environments are in essence those of single stars. In non-equal mass systems with $M_1 + M_2$ considered as fixed, the P/PT-type HZs are barely impacted compared to equal-mass systems, but higher values for $a_{\rm bin}$ are mandated for the existence of S/ST-type HZs especially for systems with high eccentricities for the binary components.

4.2 Fitting Procedure

The main aspect of this chapter concerns the derivation of fitting formulae for the existence of P/PT-type HZs and S/ST-type HZs for binary systems consisting of main-sequence stars. Through applying the least-squared method, fitting is done in two steps: first, fitting $a_{\rm bin}$ versus e_b by assuming fixed masses as reference (aimed at catching the sets of parameters where the HZs cease to exist) and, second, fitting the coefficients with stellar masses to allow the expansion of the formulae for general binary systems. In the first step, the Bayesian information criterion (BIC) and mean absolute percentage error are taken into account. The BIC is used in the second step as well for the mass fitting determination.

For P/PT-type cases, the $a_{\rm bin}$ versus e_b fitting is done using a polynomial equation, which is

$$a_{\rm bin} = \alpha_0 + \alpha_1 e_b + \alpha_2 e_b^2 \ . \tag{4.1}$$

For S/ST-type cases, the $a_{\rm bin}$ versus e_b fitting is done using a cubic equation, placed as exponent, which reads

$$a_{\rm bin} = e^{\beta_0 + \beta_1 e_b + \beta_2 e_b^2 + \beta_3 e_b^3} \ . \tag{4.2}$$

For $e_b = 0$, systems with masses of $M_1 = M_2 = 1.00\ M_\odot$ have 0.960 AU for the fitting results and 0.97 AU regarding the data for the P/PT-type GHZ, and 1.016 AU in the fitting results and 1.03 AU regarding the data for the P/PT-type RVEM to exist. For S/ST-type HZs, the fit yields 3.597 AU and 2.773 AU for the GHZ and RVEM, respectively, with data noted as 3.72 AU and 2.93 AU, respectively.

Keep e_b to be zero, systems with $M_1 = M_2 = 0.50\ M_\odot$, render 0.215 AU, 0.230 AU, 0.720 AU, and 0.568 AU in the fitting of P-GHZ, P-RVEM, S-GHZ, and S-RVEM, respectively. Conversely, the data based on the method as given in Chapter 2 are given as 0.22 AU, 0.23 AU, 0.76 AU, and 0.60 AU, respectively.

In systems with $M_1 = 1.00\ M_\odot$, $M_2 = 0.50\ M_\odot$, the fitting results read 0.805 AU, 0.850 AU, 2.702 AU, and 2.109 AU, respectively with e_b as zero for P-GHZ, P-RVEM, S-GHZ, and S-RVEM, respectively. Furthermore, 0.81 AU, 0.86 AU, 2.83 AU, and 2.23 AU are the values for corresponding data.

For the case of $M_1 = 1.25\ M_\odot$ and $M_2 = 0.75\ M_\odot$ with e_b as zero, the results for the fitting of P-GHZ, P-RVEM, S-GHZ, and S-RVEM are given as 1.185 AU, 1.253 AU, 4.229 AU, and 3.287 AU, respectively. Here the data are 1.20 AU, 1.27 AU, 4.36 AU, and 3.41 AU, respectively, again showing very close agreement. The various fitting coefficients are listed in Table 4.3.

To enhance the universal applicability of the fitting formulae, I also explored the relation between the coefficients in $a_{\rm bin}$ versus e_b fitting, and the stellar masses of the binary systems. For the coefficients in the P-type equation, α is represented by

$$\alpha_i = A_{i0} + A_{i1}M_1 + A_{i2}M_2 \tag{4.3}$$

Furthermore, for the coefficients in the S-type equation, β is represented by

$$\beta_i = B_{i0} + B_{i1}M_1 + B_{i2}M_2 + B_{i3}M_1^2 + B_{i4}M_1^3 \tag{4.4}$$

The BIC for the cases of mass fitting are listed in Table 4.4. By adding terms to the equation only containing constant and linear terms of M_1 and M_2, the BIC varies and indicates that P-type cases favor adding nothing, whereas S-type cases prefer adding M_1^2 and M_1^3, as done as part of the process. The general fitting coefficients for P-type and S-type HZs are listed in Tables 4.5 and 4.6, respectively.

Applying the calculated coefficients from stellar masses to the $a_{\rm bin}$ versus e_b equations, fitting results are plotted as well as the data for comparison (see Figure 4.2). Most of the fits are virtually indistinguishable from the data. Percent errors of the fits for selected cases are provided in Tables 4.7 and 4.8. Cases not showed here reveal similar results. In Table 4.9, the coefficients of determination measuring the goodness of the fit, are given for reference. The percentage errors are calculated as

$$\text{Percentage Error} = \left| \frac{\text{data} - \text{fitting}}{\text{data}} \right| \tag{4.5}$$

In summary, through employing a two-step fitting procedure, fully acceptable results are obtained for the fitting equations in response to the existence of GHZ and RVEM HZs depending on the system parameters (i.e., $a_{\rm bin}$, e_b, M_1, and M_2).

4.3 Applications to Observed Systems

Using the fitting formulae given above (see Equations 4.1 to 4.4), several observed binary systems have been studied in more detail to inquire on the existence of the stellar HZs, encompassing both GHZs and RVEM HZs.

Generally, the minimum $a_{\rm bin}$ for S-type HZs to exist would increase as either stellar mass increases. As for the P-type cases, the maximum $a_{\rm bin}$ is decreased with either stellar mass decreased. Thus, the maximum masses of binary components were considered for S-type HZs based on their errors for their existence, and minimum masses have been taken into account for the non-existence of HZs. In contrast, P-type HZs consider stellar minimum masses (as defined by the respective observational uncertainties) for their existence, and maximum masses for the non-existence of the HZs. As for the eccentricity, the largest eccentricity (as set by observational constraints) should be considered for the study of both S-type and P-type HZs, as it corresponds to the most adverse outcome.

4.3.1 P-type Systems

4.3.1.1 Kepler-34

Welsh et al. (2012) have reported transiting circumbinary planets both regarding Kepler-34 and Kepler-35; their study also conveys detailed information about the system's data (see Table 4.10). Kepler-34 has two Sun-like stars revolving around each in $27.7958103^{+0.0000016}_{-0.0000015}$ d, with stellar masses to be $1.0479^{+0.0033}_{-0.0030} M_{\odot}$ and 1.0208±0.0022 $M_{\odot}$, respectively. The system possesses a $0.220^{+0.011}_{-0.010} M_J$ circumbinary gas giant, i.e., somewhat less massive than Saturn, with a 1.0896 ± 0.0009 AU semi-major axis and a $0.182^{+0.016}_{-0.020}$ eccentricity. By measuring the effective temperature and metallicity of both stars, an age between 5 and 6 Gyr has been deduced (Yi et al. (2001)), based on

Yonsei–Yale theoretical models of stellar evolution, and thus the stars should still be in their main-sequence stages. The semi-major axis of the binary is $0.22882^{+0.00019}_{-0.00018}$, and the eccentricity is $0.52087^{+0.00052}_{-0.00055}$. Considering the smallest possible stellar masses and largest possible eccentricity, both P-type GHZ and P-type RVEM HZs are expected to exist, noting that those should require for $a_{\rm bin}$ to be less than 0.683 AU and less than 0.722 AU, respectively. These criteria are fulfilled based on the observational data (see Figure 4.5). Welsh et al. (2012) also pointed out that the circumbinary planet is located interior to the HZ.

4.3.1.2 Kepler-35

Kepler-35 is known to have a $0.127^{+0.020}_{-0.020} M_J$ circumbinary gas giant orbiting hosting stars on a nearly circular orbit ($e_b = 0.042^{+0.007}_{-0.004}$); see Welsh et al. (2012) for details. The planet, which has a semi-major axis to be $0.17617^{+0.00029}_{-0.00030}$ AU, is within the P-type HZs. The primary star of Kepler-35 has a mass to be $0.8877^{+0.0051}_{-0.0053} M_\odot$, and the secondary being $0.8094^{+0.0042}_{-0.0045} M_\odot$, with an orbital period of $20.733666^{+0.000012}_{-0.000012}$ days. Based on the Yonsei–Yale theoretical models of stellar evolution (Yi et al. (2001)), the age of this system is about 8 Gyr to 12 Gyr. This is larger than the solar age; however, based on the masses of the two stellar components, this system is still considered to be composed of main-sequence stars. The binary system has a semi-separation of $0.17617^{+0.00029}_{-0.00030}$ AU, and the eccentricity is given as $0.1421^{+0.0014}_{-0.0015}$. The system's semi-major axis is clearly less than the requirements for P-type HZs to exist, which are 0.674 AU and 0.712 AU for the GHZ and RVEM (see Figure 4.5). Welsh et al. (2012) pointed out that the circumbinary planet is located interior to the HZ.

4.3.1.3 Kepler-413

Following Kostov et al. (2014), Kepler-413 has a $0.820^{+0.015}_{-0.014} M_{\odot}$ K dwarf as primary, and a $0.5423^{+0.0081}_{-0.0073} M_{\odot}$ M dwarf as secondary (see Table 4.10). The two stars orbit each other on a nearly circular orbit, which has an eccentricity of $0.0365^{+0.0023}_{-0.0021}$. The orbital period is given as $10.1161114^{+0.0000099}_{-0.0000101}$ d. Kepler-413b, a $67^{+22}_{-21} M_{\oplus}$ circumbinary planet, orbiting both stars with $0.3553^{+0.0020}_{-0.0018}$ AU as semi-major axis and $0.1181^{+0.0018}_{-0.0017}$ as eccentricity, is slightly outside of the GHZ, but insight of the RVEM. Fitting with the minimum possible stellar masses and maximum possible binary eccentricity (the most adverse choices for the existence of the circumstellar HZs), the P-type GHZ and RVEM require $a_{\rm bin}$ to be smaller than 0.572 AU and 0.605 AU to allow their existence. The semi-major axis of the system is $0.10148^{+0.00057}_{-0.00052}$ AU, which satisfies the requirements for circumbinary HZs to exist (see Figure 4.5).

4.3.1.4 Kepler-1647

Following Kostov et al. (2016), Kepler-1647b has been identified a $483 \pm 206 M_{\oplus}$ gas giant in the eclipsing binary system Kepler-1647. The semi-major axis of the planet is 2.7205±0.0070 AU, which is within the P-type GHZ. The primary star is estimated to be a F8 star with stellar mass as $M_1 = 1.2207 \pm 0.0112 M_{\odot}$. The secondary star is similar to the Sun; it has a mass of $M_2 = 0.9678 \pm 0.0039 M_{\odot}$ (see Table 4.10). The estimated age of the system, identified as approximately 4.4 Gyr, corresponds to mid-age main-sequence. The binary orbital period is given as 11.2588179±0.0000013 d, with 0.1276±0.0002 AU as binary semi-major axis and 0.1602±0.0004 as binary eccentricity. Taking the largest eccentricity the smallest possible stellar masses, as conveyed by the observational results, as reference, it requires $a_{\rm bin}$ to be less than 1.037 AU for P-type GHZ to exist, and 1.096 AU for P-type

RVEM to exist. Fitting results for this system are shown in Figure 4.5, which clearly show that both the GHZ and RVEM are able to exist in this system.

4.3.2 S-type Systems

4.3.2.1 TrES-2

Following Daemgen et al. (2009), TrES-2, also known as Kepler-1, consists of a planet-hosting G0V primary star with a mass of 1.05 $M_{\odot}$. The $1.199 \pm 0.0052 M_J$ planet orbits the stellar primary based on a 0.03556 ± 0.00075 AU semi-major axis. The secondary is estimated to have a mass of 0.67 $M_{\odot}$; it is a zero-age main-sequence star. The binary separation of the system, which is estimated to be 232±12 AU, ensure that effects by the secondary star on the primary's habitable environment are largely negligible; therefore, resulting in conditions akin to a single star. Thus, S-type HZs should exist around the primary star. Although the binary eccentricity is unknown, the semi-major-axis of the binary system is larger than the required value as 23.679 AU for S-type GHZ and 19.303 AU for S-type RVEM (see Figure 4.6).

4.3.2.2 KOI-1257

Following Santerne et al. (2014), KOI-1257 consists of two main-sequence stars with stellar masses of 0.99±0.05 $M_{\odot}$ and 0.70±0.07 $M_{\odot}$, respectively (see Table 4.10). A 1.45±0.35 M_J planet is in an S-type orbit around the primary star with 0.772±0.045 as eccentricity and 0.382±0.006 AU as semi-major axis. The eccentricity of the binary system's orbit is $0.31^{+0.37}_{-0.21}$, and its semi-major axis is 5.3 AU with an uncertainty of 1.3 AU. In this system, the existence of S-type HZs strongly depends on the binary parameters, which are subject to notable uncertainties. At $e_b = 0.68$, the semi-major axis is required to be larger than 13.919 AU for an S-type GHZ and 11.019 AU for

RVEM, which means that for this value of e_b, there are no S-type HZs. However, for the smallest value of e_b, given as 0.10, the requirements for the semi-major axis now read 3.899 and 3.085 AU for the GHZ and RVEM, respectively, indicating the existence for both S-type types of HZs (see Figure 4.6). If disregarding the observational uncertainties, the semi-major axis is given as 5.3 AU. This value is larger than 5.386 AU for the S-type GHZ to exist, and larger than 4.280 AU for the S-type RVEM to exist.

4.3.3 Comparison with Other Work

I also have compared some of my results with previous work that is based on moderately different methods for the calculations of the HZ limits. For S-type and P-type HZs, this work has been given by Haghighipour et al. (2013) and Kaltenegger et al. (2013), respectively. Figure 4.7 shows the comparisons for the systems of Kepler-34, Kepler-35, Kepler-413, and KOI-1257. Comparisons between results based on GHZ and RVEM climate models are shown examples, with the observational uncertainties for the eccentricities taken into account. The percent differences are calculated as difference between habitability limits divided by the average.

Regarding Kepler-34, the luminosity of the primary is given as 1.49 $L_\odot$ and for the secondary it is 1.28 $L_\odot$. The GHZ inner limit has a percent difference between 3.04% and 3.14%, whereas the outer limit's difference varies between 0.777% and 0.780%. In case of RVEM, the inner limit has a minimum difference of 0.319% and a maximum difference of 0.321%. The values for the outer limit are given as 0.390% and 0.391%, respectively. Regarding Kepler-35, the luminosity of the primary is given as 0.94 $L_\odot$ and for the secondary it is 0.41 $L_\odot$. The GHZ inner and outer limits have minimum percent differences of 2.94% and 0.703%, and maximum percent differences of 3.08% and 0.706%, respectively. For the RVEM climate models, the

percent difference for the inner limit and outer limit are close to 0.3% and 0.5%, respectively. Regarding Kepler-413, the luminosity of the primary is given as 0.26 $L_{\odot}$ and for the secondary it is 0.03 $L_{\odot}$. The inner and outer GHZ limits have percent differences ranging from 2.82% to 3.01% and from 0.562% and 0.570%. RVEM has percent difference between 1.12% and 1.22% for the inner limits, and between 0.518% and 0.519% for the outer limits.

KOI-1257, considered as an S-type system, consists of two stars with luminosities of 1.06 $L_{\odot}$ and 0.14 $L_{\odot}$, respectively. The minimum and maximum percent differences of the GHZ inner limit are 3.22% and 3.73%, respectively. The value for the GHZ outer limit is approximately 0.75%. The RVEM inner limit is noted for having percent differences between 0.053% and 0.102%, whereas the RVEM out limit has a percentage difference of 0.43% with virtually no variation regarding the assumed eccentricity of the binary components. Therefore, in conclusion, my results on obtaining fitting formulae for the existence of S-type and P-type HZs are unaffected by the choice of habitability limits as available in the literature.

4.4 Summary and Conclusions

The aim of this chapter was the evaluation of the mathematical constraints for the possibility of HZs in stellar binary systems — an effort of interest irrespectively of hitherto planet detections in those systems. This allowed the introduction of fitting formulae that permit — in the framework of the adopted model — a straightforward "yes/no" answer whether HZs exist. The fitting formulae for the existence of the HZs, both regarding P-type and S-type HZs, obtained in this chapter relate the axes $a_{\rm bin}$ between the stellar binary components and an algebraic expansion for their orbital eccentricities; they target the limits where the respective HZs ceases to exist. For P-type cases, the attained algebraic expansion is of second order, and for S-type cases,

it is of third order, but written as an exponential exponent. The various coefficients also depend on M_1 and M_2, the masses of the stellar components, which ensures the comprehensive applicability of the fitting formulae. The current version of my methods is aimed at systems of main-sequence stars.

The stellar masses are assumed to range between 0.50 and 1.25 $M_\odot$, i.e., between spectral type M0V and F6V (e.g., Gray (2005), Mann et al. (2013)). Thus, the respective stellar luminosities range between 0.036 and 2.15 $L_\odot$. Therefore, notwithstanding late-type red dwarfs, the kind of stars for which this approach is applicable comprises more than 95% of main-sequence stars (e.g., Kroupa (2001), Kroupa (2002), Chabrier (2003)). Furthermore, detailed tests for the fitting formulae demonstrate that their accuracy compared to the exact results based on the solutions for the underlying quartic equations (see Chapter 2) is better than 5% in most cases, noting that the least accurate results are found for systems of high eccentricity, i.e., e_b greater than 0.75. In fact, for the vast majority of cases the accuracy of the fitting formulae is found to be about 1% or 2%.

This method is particularly useful for the quick assessment of observed systems with relatively large (or poorly known) uncertainties in $a_{\rm bin}$, e_b, M_1, and M_2 while noting that the latter can play a decisive role regarding whether or not S-type or P-type HZs exist. To demonstrate the applicability of this method, I explored the existence of P-type HZs for Kepler-34, Kepler-35, Kepler-413, and Kepler-1647 and S-type HZs for TrES-2 and KOI-1257. Observational uncertainties of the various system parameters have been considered as well, which can be relevant for the outcome. A good example is KOI-1257, where the existence of the S-type HZ is strongly affected by the values for both the semi-major axis and the eccentricity of the stellar motion, which are somewhat uncertain. On the other hand, I found that all P-type systems considered possess P-type HZs irrespectively of the uncertainties in the rel-

evant observational parameters. These results are also unaffected by the planetary climate models.

Generally, the likelihood for the existence of HZs is relatively high for low values of the e_b, but relatively small, or virtually non-existing, for high values of the e_b. Moreover, the likelihood if a HZs can exist is also increased if RVEM-type HZs are considered rather than GHZ-type HZs, as expected. The fact that high values for e_b decisively reduce the possibility of S-type habitability has previously been pointed out by, e.g., Cuntz (2015).

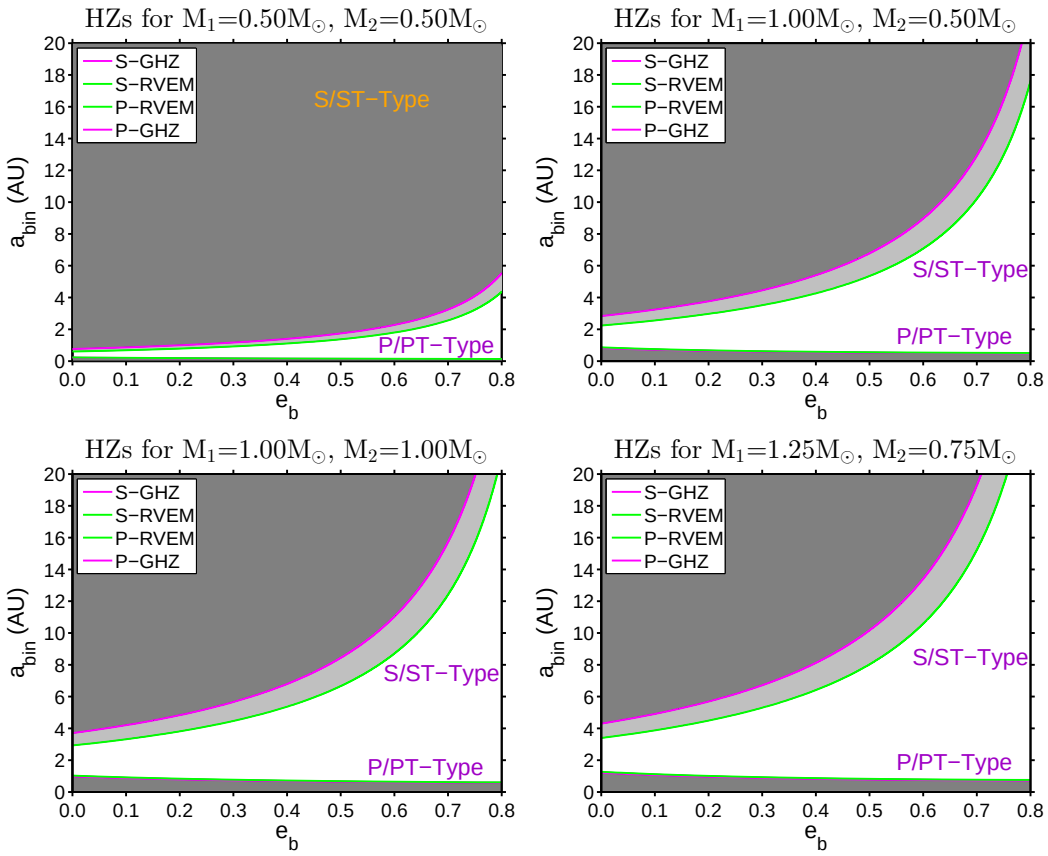

Figure 4.1 Required $a_{\rm bin}$ and e_b for the GHZ and RVEM to exist regarding selected theoretical binary systems. The GHZ can exist when the system parameters are within the gray region. System parameters fall in either gray or light gray region would allow RVEM to exist. The magenta and green curves show the critical pairs of values for the GHZ and RVEM to exist correspondingly.

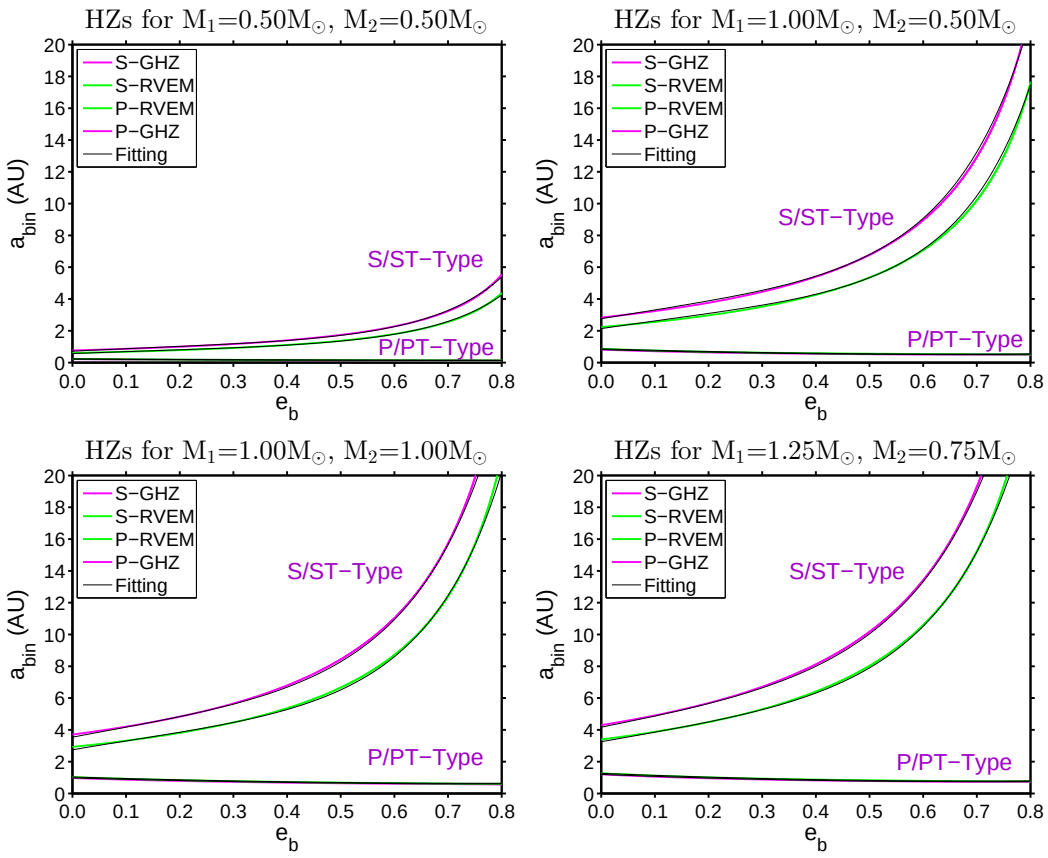

Figure 4.2 Fitting of the data for selected theoretical main-sequence stars. The magenta and green lines represent the boundaries for the GHZ and the RVEM to exist, respectively. In each subfigure, the areas beyond the magenta and green curves (top) identify the existence of the S/ST-type HZs, whereas the areas below the magenta and green curves (bottom) identify the existence of the P/PT-type HZs. The thin black curves depict the fitting results for the curve nearby, and they are virtually indistinguishable from the data curves.

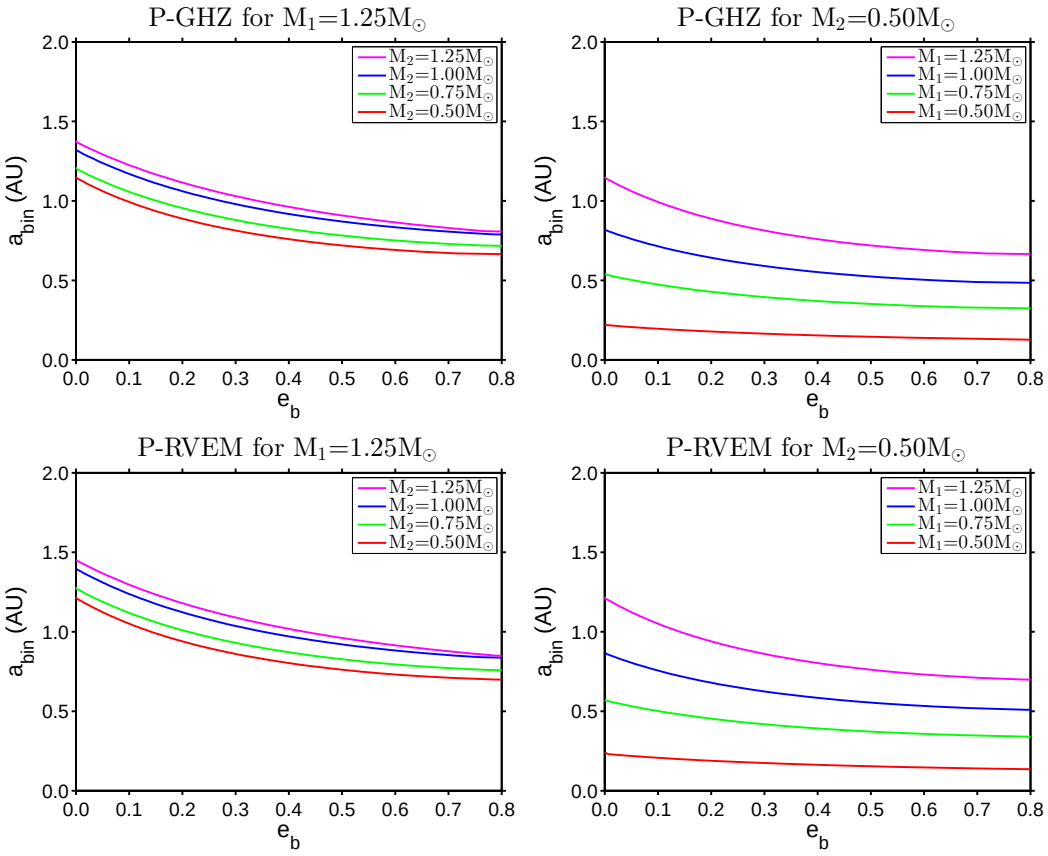

Figure 4.3 Results for P-type GHZ and RVEM. P-type HZs are realized beneath the respective curve.

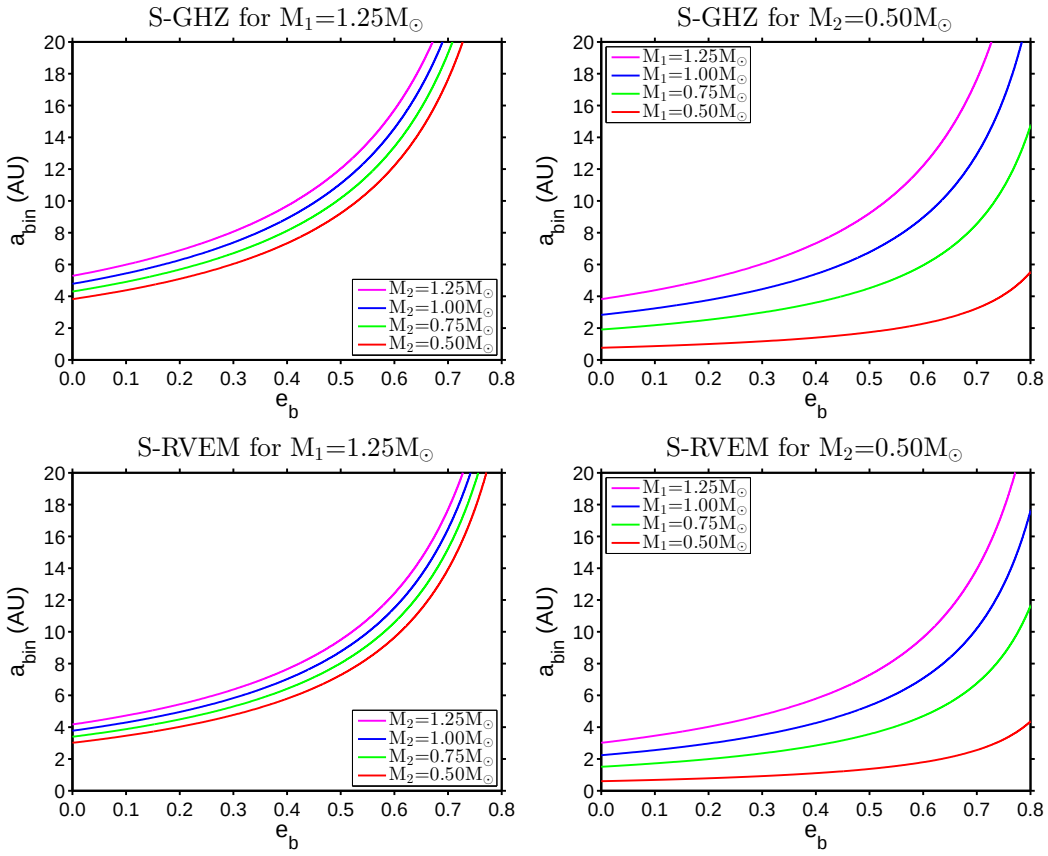

Figure 4.4 Results for S-type GHZ and RVEM. S-type HZs are realized above the respective curve.

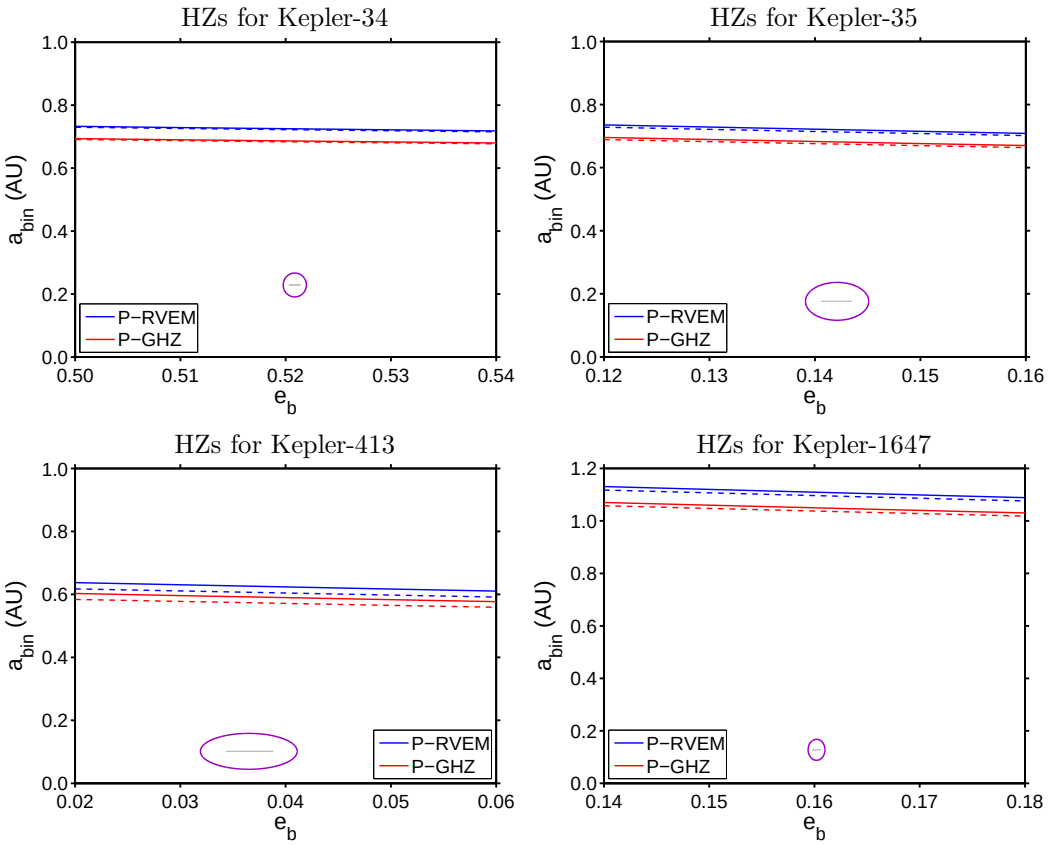

Figure 4.5 The red and blue curves are the fitting results that show the maximum $a_{\rm bin}$ for P-type HZs to exist; i.e., P-type HZs are possible below these curves. The dashed lines are the results considering the uncertainties in the stellar masses. The gray domains indicate the indicated $a_{\rm bin}$ and e_b values for the respective stellar systems with the observational uncertainties taken into account (the purple ellipses are placed to enhance the domains' visibility).

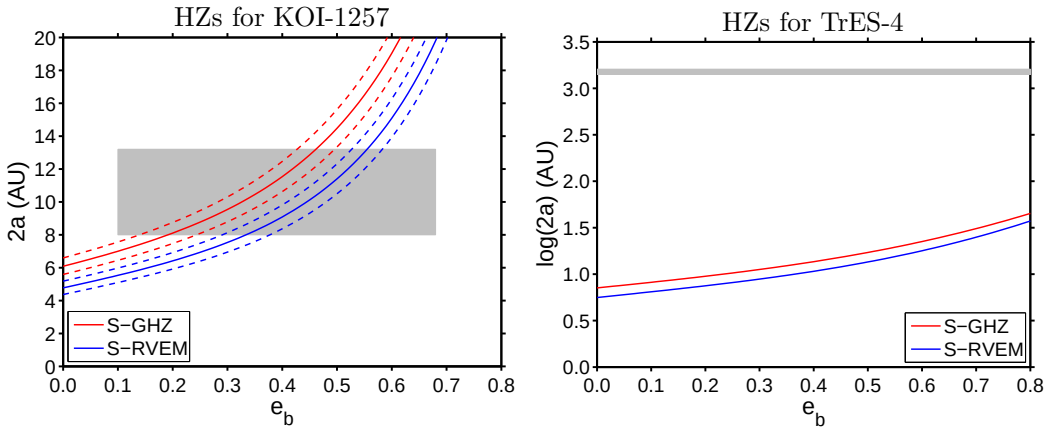

Figure 4.6 The red and blue curves are the fitting results that show the minimum $a_{\rm bin}$ for S-type HZs to exist; i.e., S-type HZs are possible above these curves. The dashed lines are the results considering the uncertainties in the stellar masses. The gray domains indicate the indicated $a_{\rm bin}$ and e_b values for the respective stellar systems with the observational uncertainties taken into account. A logarithmic scale y-scale is used for TrES-2 because of the system's very large semi-major axis.

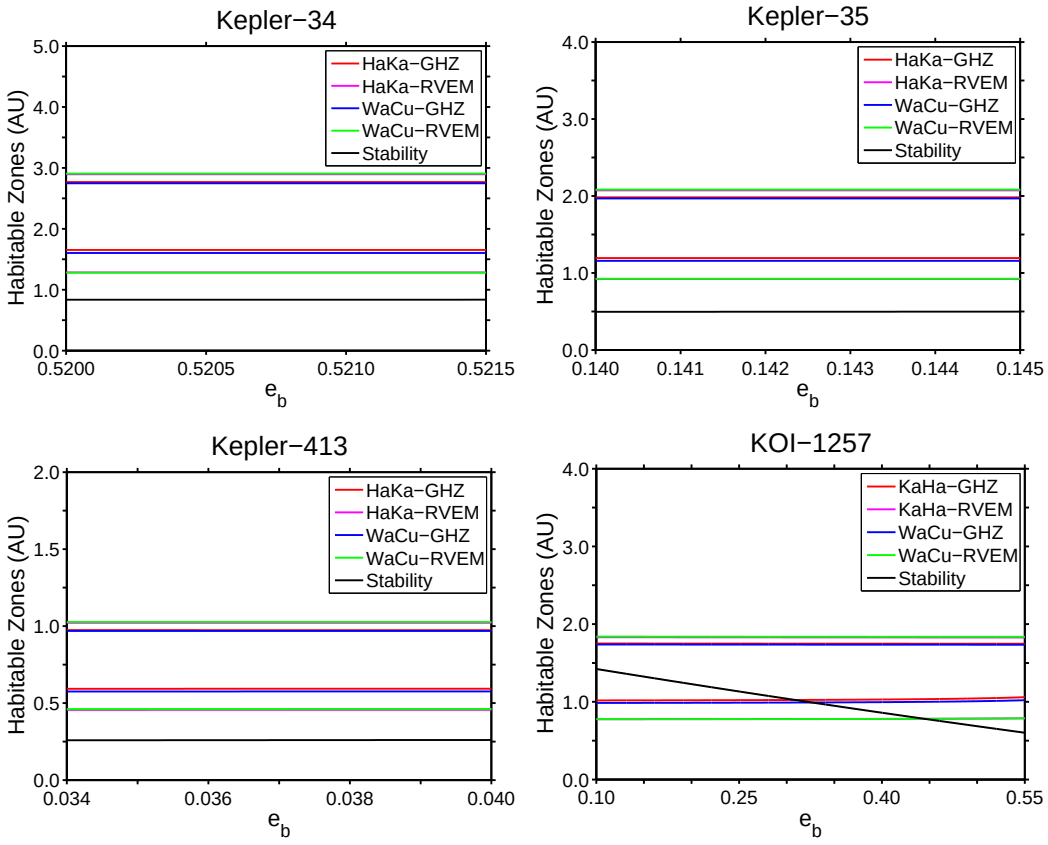

Figure 4.7 Comparisons of my results (WaCu) for Kepler-34, Kepler-35, Kepler-413, and KOI-1257 regarding the existence of HZs with previous work pertaining to the calculations of HZ limits. That work has been given by Haghighipour et al. (2013) for S-type HZs and by Kaltenegger et al. (2013) for P-type HZs, thus denoted as HaKa and KaHa, respectively. Results are given for GHZ and RVEM climate models.

Table 4.1. Stellar Parameters

M_*	Spectral Type	T_*	R_*	L_*
$(M_\odot)$	...	(K)	$(R_\odot)$	$(L_\odot)$
1.25	∼F6V	6257	1.253	2.154
1.00	∼G2V	5780	1.000	1.0000
0.75	∼K2V	5104	0.766	0.3568
0.50	∼M0V	3664	0.472	0.03593

Note. — Adopted from Cuntz (2014) and Cuntz (2015).

Table 4.2. BIC Values for $a_{\rm bin}$ versus e_b Fitting

BIC	Linear	Quadratic	Cubic	Quartic
P−GHZ	−287.28	−418.18	−538.74	−627.83
P−RVEM	−295.91	−432.93	−564.12	−642.10
S−GHZ	−7915.7	−12327	−16347	−19794
S−RVEM	−7422.6	−11599	−15395	−18840

Note. — The case of $M_1 = M_2 = 1.0\ M_\odot$ is given as an example for the determination of the $a_{\rm bin}$ versus e_b fitting. For all S-type results, the logarithm of $a_{\rm bin}$ is applied. The mean absolute percentage error (MAPE) is calculated as well, and a 2% threshold is used. The BICs are found to decrease as the orders of the equations increase from 1 to 3 for all cases indicating that it is acceptable to have cubic equations. Lowest order equations satisfy the MAPE requirement are chosen for less complexity.

Table 4.3. Fitting Coefficients

Model	Coefficient	Case 1	Case 2	Case 3	Case 4
P-GHZ	α_0	0.215	0.805	0.805	1.185
...	α_1	-0.205	-0.933	-0.933	-1.302
...	α_2	0.123	0.716	0.716	0.949
P-RVEM	α_0	0.230	0.850	0.850	1.253
...	α_1	-0.228	-0.957	-0.957	-1.371
...	α_2	0.146	0.695	0.695	0.992
S-GHZ	β_0	-0.328	0.994	0.994	1.442
...	β_1	2.169	2.088	2.088	1.601
...	β_2	-3.046	-2.497	-2.497	-0.956
...	β_3	4.346	3.901	3.901	2.506
S-RVEM	β_0	-0.566	0.746	0.746	1.19
...	β_1	2.177	2.256	2.256	1.844
...	β_2	-3.065	-3.024	-3.024	-1.787
...	β_3	4.359	4.349	4.349	3.275

Note. — Case 1: $M_1 = M_2 = 0.50\ M_\odot$; Case 2: $M_1 = 1.00\ M_\odot$, $M_2 = 0.50\ M_\odot$; Case 3: $M_1 = M_2 = 1.00\ M_\odot$; Case 4: $M_1 = 1.25\ M_\odot$, $M_2 = 0.75\ M_\odot$.

Table 4.4. BIC Values for Mass Fitting

Model	BIC	Linear to M_1 and M_2	Adding M_1^2 and M_2^2	Adding M_1M_2 and M_1^2	Adding M_1M_2 and M_2^2	Adding M_1^2 and M_1^3	Adding M_2^2 and M_2^3
P−GHZ	Constant	−80.90	−75.94	−76.06	−75.21	**−81.84**	−75.94
...	Coef. of e_b term	**−71.59**	−67.34	−68.70	−68.32	−70.66	−67.67
...	Coef. of e_b^2 term	**−74.75**	−69.81	−71.19	−70.77	−74.42	−69.65
P−RVEM	Constant	**−78.20**	−71.14	−75.24	−75.76	−76.26	−74.80
...	Coef. of e_b term	−68.41	−66.79	**−68.86**	−64.14	−65.96	−63.09
...	Coef. of e_b^2 term	−64.78	**−66.50**	−63.89	−65.04	−61.58	−63.44
Total	...	**−438.64**	−417.51	−423.94	−419.25	−430.73	−414.59
S−GHZ	Constant	−31.68	−48.70	−49.40	−34.20	**−66.87**	−28.96
...	Coef. of e_b term	−41.16	−51.60	−51.75	−38.90	**−57.37**	−37.18
...	Coef. of e_b^2 term	−18.43	−30.32	−30.15	−17.85	**−35.97**	−14.79
...	Coef. of e_b^3 term	−20.18	−34.76	−34.62	−20.22	**−39.84**	−16.63
S−RVEM	Constant	−31.78	−46.96	−47.44	−33.85	**−69.32**	−28.97
...	Coef. of e_b term	−36.27	−53.25	−54.17	−38.71	**−65.40**	−33.20
...	Coef. of e_b^2 term	−13.49	−28.14	−30.12	−17.55	**−36.86**	−10.94
...	Coef. of e_b^3 term	−16.11	−30.85	−32.98	−20.42	**−39.04**	−13.67
Total	...	−209.11	−324.58	−330.62	−221.70	**−410.68**	−184.34

Note. — The coefficients from the $a_{\rm bin}$ versus e_b fitting are further fitted based on an equation linear in the stellar masses. Additional terms are added by checking the BIC. The smallest BIC in each line is given in bold font. The total BIC values in each column are compared. For P-type, adding nothing is preferred, whereas for S-type, adding M_1^2 and M_1^3 turns out to be the best choice.

Table 4.5. General Fitting Coefficients, P-Type

Model	Coefficient	A_{i0}	A_{i1}	A_{i2}
P-GHZ	α_0	-0.541	1.201	0.318
...	α_1	0.541	-1.504	0.012
...	α_2	-0.345	1.219	-0.275
P-RVEM	α_0	-0.570	1.266	0.338
...	α_1	0.578	-1.553	-0.036
...	α_2	-0.384	1.213	-0.187

Table 4.6. General Fitting Coefficients, S-Type

Model	Coefficient	B_{i0}	B_{i1}	B_{i2}	B_{i3}	B_{i4}
S-GHZ	β_0	−5.871	16.88	0.499	−14.932	4.688
...	β_1	−0.002	8.934	−0.464	−9.835	3.160
...	β_2	2.852	−24.115	1.018	26.776	−8.352
...	β_3	−0.414	19.528	−0.991	−21.219	6.371
S-RVEM	β_0	−6.354	17.873	0.500	−16.177	5.168
...	β_1	3.311	−4.510	−0.461	7.080	−3.349
...	β_2	−7.312	17.184	0.954	−25.04	11.499
...	β_3	8.047	−14.891	−0.883	21.811	−10.027

Table 4.7. Errors of Fitting

e_b	$M_1 = M_2 = 1.00\ M_\odot$				$M_1 = 1.00\ M_\odot, M_2 = 0.50\ M_\odot$			
...	P-GHZ	P-RVEM	S-GHZ	S-RVEM	P-GHZ	P-RVEM	S-GHZ	S-RVEM
0.0	0.53%	0.17%	4.96%	6.36%	0.58%	0.02%	2.71%	4.09%
0.1	2.28%	2.21%	0.67%	0.44%	2.25%	2.20%	2.21%	2.46%
0.2	2.66%	2.46%	0.11%	0.89%	2.27%	2.33%	3.26%	4.09%
0.3	2.20%	2.04%	0.70%	0.09%	1.31%	1.38%	2.14%	2.80%
0.4	1.59%	1.40%	1.59%	1.52%	0.33%	0.19%	0.66%	0.86%
0.5	1.27%	1.11%	1.82%	2.20%	0.07%	0.40%	0.18%	0.20%
0.6	1.59%	1.50%	0.98%	1.40%	1.20%	0.16%	1.13%	0.62%
0.7	2.99%	2.98%	0.67%	0.08%	4.13%	2.32%	2.27%	2.59%
0.8	5.78%	5.82%	...	...	9.26%	6.34%	...	0.92%

Table 4.8. Errors of Fitting, Continued

e_b	$M_1 = 0.75\ M_\odot, M_2 = 0.50\ M_\odot$				$M_1 = M_2 = 0.50\ M_\odot$			
...	P-GHZ	P-RVEM	S-GHZ	S-RVEM	P-GHZ	P-RVEM	S-GHZ	S-RVEM
0.0	3.48%	3.47%	2.97%	3.36%	0.33%	0.00%	5.41%	6.08%
0.1	1.87%	1.85%	3.77%	3.80%	1.82%	2.05%	0.58%	0.59%
0.2	2.02%	1.95%	5.40%	5.52%	2.50%	2.74%	2.30%	2.26%
0.3	2.96%	2.92%	4.04%	4.12%	2.37%	2.53%	1.21%	1.09%
0.4	3.99%	4.14%	1.91%	2.12%	2.00%	1.94%	0.65%	0.75%
0.5	4.38%	4.83%	0.87%	0.98%	1.80%	1.49%	1.60%	1.59%
0.6	3.58%	4.52%	1.63%	1.63%	2.25%	1.47%	0.67%	0.65%
0.7	1.29%	2.88%	3.43%	3.34%	3.60%	2.33%	1.24%	1.12%
0.8	2.58%	0.45%	0.34%	0.46%	6.10%	4.56%	2.27%	2.86%

Table 4.9. Coefficient of Determination

Systems	P-GHZ	P-RVEM	S-GHZ	S-RVEM
$M_1 = 1.25\ M_\odot, M_2 = 1.25\ M_\odot$	0.9976	0.9975	0.9967	0.9969
$M_1 = 1.25\ M_\odot, M_2 = 1.00\ M_\odot$	0.9795	0.9758	0.9999	0.9997
$M_1 = 1.25\ M_\odot, M_2 = 0.75\ M_\odot$	0.9919	0.9929	0.9990	0.9991
$M_1 = 1.25\ M_\odot, M_2 = 0.50\ M_\odot$	0.9954	0.9940	0.9991	0.9990
$M_1 = 1.00\ M_\odot, M_2 = 1.00\ M_\odot$	0.9803	0.9820	0.9990	0.9984
$M_1 = 1.00\ M_\odot, M_2 = 0.75\ M_\odot$	0.9970	0.9963	0.9994	0.9988
$M_1 = 1.00\ M_\odot, M_2 = 0.50\ M_\odot$	0.9849	0.9853	0.9985	0.9978
$M_1 = 0.75\ M_\odot, M_2 = 0.75\ M_\odot$	0.9876	0.9861	0.9947	0.9954
$M_1 = 0.75\ M_\odot, M_2 = 0.50\ M_\odot$	0.9619	0.9632	0.9960	0.9962
$M_1 = 0.50\ M_\odot, M_2 = 0.50\ M_\odot$	0.9780	0.9834	0.9991	0.9991

Table 4.10. System Parameters

System	M_1	M_2	$a_{\rm bin}$	e_b	Reference
...	($M_\odot$)	($M_\odot$)	(AU)	...	...
Kepler-34	$1.0479^{+0.0033}_{-0.0030}$	1.0208±0.0022	$0.22882^{+0.00019}_{-0.00018}$	$0.52087^{+0.00052}_{-0.00055}$	Welsh et al. (2012)
Kepler-35	$0.8877^{+0.0051}_{-0.0053}$	$0.8094^{+0.0042}_{-0.0045}$	$0.17617^{+0.00029}_{-0.00030}$	$0.1421^{+0.0014}_{-0.0015}$	Welsh et al. (2012)
Kepler-413	$0.820^{+0.015}_{-0.014}$	$0.5423^{+0.0081}_{-0.0073}$	$0.10148^{+0.00057}_{-0.00052}$	$0.0365^{+0.0023}_{-0.0021}$	Kostov et al. (2014)
Kepler-1647	1.2207±0.0112	0.9678±0.0039	0.1276±0.0002	0.1602±0.0004	Kostov et al. (2016)
TrES-2	1.05	0.67	232±12	...	Daemgen et al. (2009)
KOI-1257	0.99±0.05	0.70±0.07	5.3±1.3	$0.31^{+0.37}_{-0.21}$	Santerne et al. (2014)

CHAPTER 5

Summary and Future Work

Stellar HZs are calculated following the comprehensive mathematical approach from Cuntz (2014, 2015). This includes (1) the consideration of a joint constraint including orbital stability and a habitable region for a putative system planet through the stellar radiative energy fluxes needs to be met; (2) applications to stellar systems in either circular or elliptical orbits. The inspection of the planetary orbital stability limits follows the work by Holman & Wiegert (1999), which expands on previous results including work by Dvorak (1986) and Rabl & Dvorak (1988).

In Chapter 3, comparisons are made among HZs based on different planetary climate models, which show great difference in inner limits of HZs between results adopting model from Selsis et al. (2007) and Kopparapu et al. (2014). Furthermore, in Chapter 4, fitting formulae are derived based on the updated planetary climate mode from Kopparapu et al. (2014), aiming at the quick determination of the possibility of HZs in stellar binary systems consist main-sequence stars, with detailed consideration of observational uncertainties. The fitting formulae have also been applied to real systems.

My future work will consider stellar systems of stars other than main-sequence components and also take into account future advances about planetary climate models, including the impact of planetary masses and atmospheric structures. I am also going to further investigate the effects of secondary stars on HZs in P-type systems, with the consideration of different stellar parameters. Additional work will include cases where the planet temporarily leaves the HZ (see, e.g., Eggl et al. (2012),

Williams & Pollard (2002) for previous results) as well as higher-order systems with more than two stellar components, e.g., Proxima Centauri (Anglada-Escudé et al. (2016)).

Bibliography

Anglada-Escudé, G., Amado, P. J., Barnes, J., et al. 2016, Nature, 536, 437

Bazsó, Á., Pilat-Lohinger, E., Eggl, S., et al. 2017, MNRAS, 466, 1555

Bennett, D. P., Rhie, S. H., Udalski, A., et al. 2016, AJ, 152, 125

Borucki, W. J., Agol, E., Fressin, F., et al. 2013, Science, 340, 587

Chabrier, G. 2003, PASP, 115, 763

Cuntz, M. 2014, ApJ, 780, 14

Cuntz, M. 2015, ApJ, 798, 101

Cuntz, M., & Bruntz, R. 2014, in Cool Stars, Stellar Systems, and the Sun: 18th Cambridge Workshop, ed. G. van Belle & H. Harris (Flagstaff: Lowell Observatory), p. 831

Daemgen, S., Hormuth, F., Brandner, W., et al. 2009, A&A, 498, 567

Duchêne, G., & Kraus, A. 2013, ARAA, 51, 269

Duquennoy, A., & Mayor, M. 1991, A&A, 248, 485

Dvorak, R. 1982, OAWMN, 191, 423

Dvorak, R. 1986, A&A, 167, 379

Eggenberger, A., Udry, S., & Mayor, M. 2004, A&A, 417, 353

Eggl, S., Pilat-Lohinger, E., Georgakarakos, N., et al. 2012, ApJ, 752, 74

Fischer, E., Martínez, G. M., Elliott, H .M., et al. 2014, GeoRL, 41, 4456

Forget, F., Pierrehumbert, R. T. 1997, Science, 278, 1273

Gray, D. F. 2005, The Observation and Analysis of Stellar Photospheres, 2nd edn. (Cambridge: Cambridge University Press)

Gillon, M., Triaud, A. H. M. I., Demory, B., et al. 2017, Nature, 542, 456

Haghighipour, N. 2008, in Exoplanets, Springer Praxis Books, Chichester, UK, p. 223

Haghighipour, N., Dvorak, R., & Pilat-Lohinger, E. 2010, ASSL, 366, 285

Haghighipour, N., & Kaltenegger, L. 2013, ApJ, 777, 166;

Hart, M. H. 1978, Icarus, 33, 23

Holman, M. J., & Wiegert, P. A. 1999, AJ, 117, 621

Huang, S. S. 1959, AmSci, 47, 397

Jenkins, J. M., Twicken, J. D., Batalha, N. M., et al. 2015, AJ, 150, 56

Kane, S. R., & Hinkel, N. R. 2013, ApJ, 762, 7

Kane, S. R., Hill, M. L., Kasting, J. F. 2016, ApJ, 830, 1

Kaltenegger, L., & Haghighipour, N. 2013, ApJ, 777, 165

Kasting, J. F., Whitmire, D. P., & Reynolds, R. T. 1993, Icarus, 101, 108

Kopparapu, R. K., Ramirez, R., Kasting, J. F., et al. 2013, ApJ, 765, 131; Erratum 770, 82

Kopparapu, R. K., Ramirez, R. M., SchottelKotte, J., et al. 2014, ApJ, 787, L29

Kostov, V. B., McCullough, P. R., Carter, J. A., et al. 2014, ApJ, 784, 14; Erratum 787, 93

Kostov, V. B., Orosz, J. A., Welsh, W. F., et al. 2016, ApJ, 827, 86

Kroupa, P. 2001, MNRAS, 322, 231

Kroupa, P. 2002, Science, 295, 82

Latham, D. W., Stefanik, R. P., Mazeh, T., et al. 1989, Nature, 339, 38

Ma, B., Ge, J., Wolszczan, A., et al. 2016, AJ, 152, 112

Mann, A. W., Gaidos, E., & Ansdell, M. 2013, ApJ, 779, 188

Milone, A. P., Marino, A. F., D'Antona, F., et al. 2016, MNRAS, 458, 4368

Mischna, M. A., Kasting, J. F., Pavlov, A., & Freedman, R. 2000, Icarus, 145, 546

Müller, T. W. A., & Haghighipour, N. 2014, ApJ, 782, 26

Ortiz, M., Gandolfi, D., Reffert, S., et al. 2015, A&A, 573, L6

Patience, J., White, R. J., Ghez, A. M., et al. 2002, ApJ, 581, 654

Pilat-Lohinger, E., & Dvorak, R. 2002, CMDA, 82, 143

Pollack, J. B., Kasting, J. F., Richardson, S. M., & Poliakoff, K. 1987, Icarus, 71, 203

Quintana, E. V. 2008, ASPC, 398, 201

Rabl, G., & Dvorak, R. 1988, A&A, 191, 385

Raghavan, D., Henry, T. J., Mason, B. D., et al. 2006, ApJ, 646, 523

Raghavan, D., McAlister, H. A., Henry, T. J., et al. 2010, ApJ, 190, 1

Roell, T., Neuhäuser, R., Seifahrt, A., & Mugrauer, M. 2012, A&A, 542, A92

Santerne, A., Hébrard, G., Deleuil, M., et al. 2014, A&A, A571, 37

Santerne, A., Hébrard, G., Lillo-Box, J., et al. 2016, ApJ, 824, 55

Selsis, F., Kasting, J. F., Levrard, B., et al. 2007, A&A, 476, 1373

Sigurdsson, S., Richer, H. B., Hansen, B. M., et al. 2003, Science, 301, 193

Solomon, S. C., Head, J. W. 1991, Science, 252, 252

Underwood, D. R., Jones, B. W., & Sleep, P. N. 2003, IJAsB, 2, 289

Wang, Zh., & Cuntz, M. 2016, in The 19th Cambridge Workshop on Cool Stars, Stellar Systems, and the Sun, Uppsala, Sweden, June 6-10, 2016, ZENODO, id. 7

Welsh, W. F., Orosz, J. A., Carter, J. A., et al. 2012, Nature, 481, 475

Wolszczan, A., & Frail, D. A. 1992, Nature, 355, 145

Welsh, W. F., Orosz, J. A., Short, D. R., et al. 2015, ApJ, 809, 26

Williams, D. M., & Pollard, D. 2002, IJAsB, 1, 61

Yi, S., Demarque, P., Kim, Y.-C., et al. 2001, ApJ, 136, 417

Zuluaga, J. I., Mason, P. A., & Cuartas-Restrepo, P. A. 2016, ApJ, 818, 160

BIOGRAPHICAL STATEMENT

Zhaopeng Wang was born in Tianjin, China, in 1989. He received his B.S. degree from Nankai University, China, in 2009, his M.S. and Ph.D. degrees from The University of Texas at Arlington in 2014 and 2017, respectively, all in Physics. His current research interest is in the area of habitability in single-star and higher-order systems. He is a member of the American Astronomical Society.